

Modeling and Analysis of Mixed Flow of Cars and Powered Two Wheelers

Sosina Gashaw[†], Paola Goatin[‡], Jérôme Härri[†]

[†]*EURECOM, Communication System Department, Sophia Antipolis*

[‡]*Université Côte d’Azur, Inria, CNRS, LJAD, France*

Abstract

In modern cities, a rapid increase of motorcycles and other types of Powered Two-Wheelers (PTWs) is observed as an answer to long commuting in traffic jams and complex urban navigation. Such increasing penetration rate of PTWs creates mixed traffic flow conditions with unique characteristics that are not well understood at present. Our objective is to develop an analytical traffic flow model that reflects the mutual impacts of PTWs and Cars. Unlike cars, PTWs filter between cars, have unique dynamics, and do not respect lane discipline, therefore requiring a different modeling approach than traditional “Passenger Car Equivalent” or “Follow the Leader”. Instead, this work follows an approach that models the flow of PTWs similarly to a fluid in a porous medium, where PTWs “percolate” between cars depending on the gap between them.

Our contributions are as follows: (I) a characterization of the distribution of the spacing between vehicles by the densities of PTWs and cars; (II) a definition of the equilibrium speed of each class as a function of the densities of PTWs and cars; (III) a mathematical analysis of the model’s properties (IV) an impact analysis of the gradual penetration of PTWs on cars and on heterogeneous traffic flow characteristics.

Keywords: Multiclass traffic flow model, Powered two wheelers, Porous flow, Traffic impacts analysis

1. Introduction

2 While a car is seen as a social achievement in most of the eastern coun-
3 tries, drivers in Europe slowly replace them with motorcycles and other types

4 of Powered Two-Wheeler (PTW) to mitigate their perceived impact of traffic
5 congestion (e.g. reduced travel time). In some cities, electrical scooter shar-
6 ing initiatives are also proposed for drivers to switch transportation modes
7 when reaching city centers. The significantly growing use of PTWs calls for
8 new technologies to integrate PTWs safely and efficiently with other road
9 users. Thus far, the focus is mainly on solving the safety issues of PTWs.
10 However, the other aspect, i.e. traffic flow efficiency, has not been addressed
11 sufficiently. Emerging intelligent transport system (ITS) technologies would
12 play an important role in improving traffic mobility of PTWs as well as other
13 users. This would be achieved by reducing the influence of PTWs on other
14 road users, for example at intersections. Additionally, the opportunity pro-
15 vided by PTWs could be exploited effectively by introducing a cooperation
16 between PTWs and other interacting vehicles. Other 'PTWs aware' tech-
17 nologies could also contribute to promote PTWs use, which in turn minimize
18 congestion.

19 Yet, PTWs create traffic flow effects Yet, PTWs create traffic flow effects
20 (e.g. car flow reduction in presence of PTWs, PTW filtering between and up
21 car streams, etc...) that are difficult to understand with the currently avail-
22 able models. Without such understanding, it is difficult to evaluate or develop
23 innovative transportation solutions with or for PTWs, such as adapting traf-
24 fic lights management to mixed traffic, safety-related PTW applications such
25 as collision/approach warnings, or multi-modal initiatives.

26 The interaction between PTWs and cars creates mixed traffic flow situa-
27 tions, for which state-of-art models are not adapted. Multi-class flow mod-
28 eling arises as an effort to characterize such mixed traffic flow situations,
29 which may be characterized roughly in two domains: Mixed "driver" char-
30 acteristics (Daganzo, 2002) or mixed "vehicle" characteristics. In this work,
31 we focus on the latter case, where a classification among the vehicle classes
32 is made on lane specific patterns, vehicles physical and dynamical features,
33 and where each vehicle in a class possesses identical characteristics (Logghe
34 and Immers, 2008).

35 In a microscopic approach, the heterogeneity of driver and vehicle char-
36 acteristics is modeled by defining different behavioral rules and parameters
37 such as longitudinal and lateral movement rule (Pandey et al., ???), speed
38 choice, headway (Lenorzer et al., 2015), reaction time, etc. The parameters
39 and driver behaviors are described differently depending on the interacting
40 vehicle classes (SHIOMI et al., 2012). Space discretization methods are also
41 introduced to accommodate lateral movement within a lane and the variation

42 in vehicle size (Chen et al., 2013; Mathew et al., 2013).

43 Multi-class traffic flows are usually evaluated following a metric called
44 “Passenger Car Equivalent” (PCE), which reports the impact of a given
45 class of traffic on traffic flow variables. With PCE a heterogeneous traffic
46 flow is converted to a hypothetical homogeneous flow by representing the
47 influence of each vehicle in terms of the equivalent number of passengers per
48 car. PCE value for vehicles varies with the traffic conditions (Praveen and
49 Arasan, 2013) and the value should be selected depending on traffic speed,
50 vehicles’ size, headway and other traffic variables (Adnan, 2014). However,
51 only few models Van Lint et al. (2008) define traffic state dependent PCE
52 value.

53 Numerous multi-class models are stemmed from the desire to characterize
54 mixed flows of cars and trucks. For instance, the model in (Zhang and Jin,
55 2002) formulates a mixed flow of passenger cars and trucks based on their
56 free flow speed difference. A two-class flow model proposed in (Chanut and
57 Buisson, 2003) differentiates vehicles according to their length and speed.
58 Furthermore, heterogeneity among vehicles is modeled relating to maximal
59 speed, length and minimum headway of vehicles in (Van Lint et al., 2008).
60 Despite providing a separate representation for each vehicle classes, in all
61 these models (Chanut and Buisson, 2003; Van Lint et al., 2008; Zhang et al.,
62 2006) vehicle classes have identical critical and jam density parameters, but
63 the parameters are scaled according to the actual traffic state. The multi-
64 class model in (Wong and Wong, 2002) extends LWR model for heterogeneous
65 drivers by distinguishing the vehicle classes by the choice of the speed. The
66 assumption is that drivers respond in a different way to the same traffic
67 density. Correspondingly, the work in (Benzoni-Gavage and Colombo, 2003)
68 presents a mixed flow for several populations of vehicles, where the vehicle
69 classes are differentiated by the maximal speed, and the equilibrium speed
70 is expressed as a function of total occupied space. The model in (Fan and
71 Work, 2015) uses a similar approach, yet integrating a specific maximum
72 occupied space for each vehicle class.

73 Mixed flows consisting of PTWs yet exhibit distinctive features from the
74 assumption taken in the previously described multi-class models, making
75 them look more like disordered flows without any lane rule. Their narrow
76 width indeed grants PTWs flexibility to share lanes with other vehicles or
77 filter through slow moving or stationary traffic, requiring traffic stream at-
78 tributes to be defined differently from traffic following lane rules (Mallikar-
79 juna and Rao, 2006). Accordingly, Nair et al. (2011) proposed to model

80 PTWs as a fluid passing through a porous medium. The speed-density re-
81 lationship is presented in terms of pore size distributions, which Nair et al.
82 obtained through exhaustive empirical simulations. This approach is com-
83 putational very expensive and hardly reproducible, as it requires a different
84 set up for each scenario being considered. On a later work from the same
85 authors (Nair et al., 2012), the pore size distribution is assumed to follow
86 an exponential distribution. Yet, the distribution parameter λ is defined
87 wrongly, i.e. the mean pore size increases with increasing of vehicle class
88 densities. Furthermore, the mean pore size is not described uniquely for
89 given vehicle-classes densities.

90 Therefore, this paper focuses specifically on a more realistic modeling of
91 the pore size distribution, which is critical to mixed flow models based on a
92 porous medium strategy. Our first contribution provides an enhanced mixed
93 flow modeling, where we: (i) provide a closed form analytical expression
94 for the pore size distribution and the statistical parameters of the pore size
95 distribution (mean, variance and standard deviation) for generic traffic flow
96 consisting of cars and PTWs; (ii) propose a fundamental relation described as
97 a function of the density of each vehicle class. The fundamental diagram and
98 the parameters for the fundamental diagram are defined uniquely for each
99 class, and are also adapted to the traffic condition; (iii) Provide a mathemat-
100 ical analysis of the model's properties (iv) apply a consistent discretization
101 method for the approximation of the conservation equations. Our second
102 contribution evaluates the impact of our enhanced model to traffic flow char-
103 acteristics, where we: (i) evaluate the impact of the maximum road capacity;
104 (ii) formulate mixed flow travel time; (iii) analyze traffic light clearance time,
105 and this considering a gradual increase of PTWs.

106 The proposed model contributes as an enabler for 'PTW aware' emerging
107 technologies and traffic regulations. For example, a variety of traffic control
108 strategies require traffic flow models to predict the traffic state and make an
109 appropriate control decision. Employing our model in such system opens a
110 door to the inclusion of PTWs in traffic control. On the other hand, the
111 model can be used as a framework to assess the optimality of the existing
112 control schemes, including information collection and computation methods.
113 Moreover, the model could help traffic regulator to determine collective and
114 class-specific optima and to induce a vehicle class specific flow adjustment.
115 In this way, new traffic regulations adapted to PTWs can be introduced,
116 which in turn promotes the use of PTWs. Additionally, our model could
117 be applied to design a smart two-wheeler navigation system which is well

118 aware of PTWs' capability to move through congested car traffic and pro-
 119 vides a route plan accordingly. The model could also contribute in the proper
 120 integration of PTWs into multi-modal transport planning. In general, the
 121 model plays a role in enabling 'PTW aware' traffic efficiency related appli-
 122 cations/technologies.

123 2. Model description

124 One of the most used macroscopic models is the first order model de-
 125 veloped by Lighthill, Whitham and Richards (Lighthill and Whitham, 1955;
 126 Richards, 1956). In the LWR model, traffic flow is assumed to be analogous
 127 to one-directional fluid motion, where macroscopic traffic state variables are
 128 described as a function of space and time. Mass conservation law and the
 129 fundamental relationship of macroscopic state variables, namely, speed, den-
 130 sity, and flow are the basic elements for LWR formulation. The conservation
 131 law says that with no entering or leaving vehicles the number of vehicles
 132 between any two points is conserved. Thus, the first order PDE equation
 133 based on the conservation law takes the form

$$\frac{\partial \rho(x, t)}{\partial t} + \frac{\partial q(x, t)}{\partial x} = 0, \quad (1)$$

134 where $\rho(x, t), q(x, t)$ are, respectively, the density and the flow of cars at
 135 position x and time t . Flow $q(x, t)$ is expressed as function of the traffic
 136 state variables:

$$q(x, t) = \rho(x, t)v(x, t) \quad (2)$$

137 The speed $v(x, t)$ depends on the density and a unique speed value corre-
 138 sponds to a specific traffic density, i.e.

$$v(x, t) = V(\rho(x, t)).$$

139 In the original LWR model, all vehicles in a traffic stream are consid-
 140 ered to exhibit similar characteristics. Therefore, no classification is made
 141 between vehicle classes. Multi-class extensions of the LWR model emerge to
 142 accommodate the heterogeneity in many aspects of road users. In multi-class
 143 modeling, vehicles with identical characteristics are grouped into a class and
 144 a conservation law applies to each class. For two vehicle classes the conser-
 145 vation equation is written as

$$\frac{\partial \rho_i(x, t)}{\partial t} + \frac{\partial q_i(x, t)}{\partial x} = 0, \quad i = 1, 2, \quad (3)$$

146 where ρ_i and q_i denote density and flow of class i , respectively. Class specific
 147 flow, speed and density are related by the equations

$$q_i(x, t) = \rho_i(x, t)v_i(x, t), \quad i = 1, 2. \quad (4)$$

148 The equilibrium speed v_i for the individual vehicle class i is a function of the
 149 densities of both classes and satisfies the following conditions:

$$v_i = V_i(\rho_1, \rho_2), \quad \partial_1 V_i(\rho_1, \rho_2) \leq 0, \quad \partial_2 V_i(\rho_1, \rho_2) \leq 0, \quad (5)$$

150 where $\partial_1 V_i(\rho_1, \rho_2)$ and $\partial_2 V_i(\rho_1, \rho_2)$ denote $\frac{\partial V_i(\rho_1, \rho_2)}{\partial \rho_1}$ and $\frac{\partial V_i(\rho_1, \rho_2)}{\partial \rho_2}$, respectively.
 151 The interaction among vehicle classes is captured through the equilibrium
 152 speed. Moreover, the equilibrium speed is uniquely defined for all points of
 153 the space

$$S = \{(\rho_1, \rho_2) : \rho_1 \leq \rho_1^{jam}(\rho_2), \rho_2 \leq \rho_2^{jam}(\rho_1)\} \quad (6)$$

154 where $\rho_1^{jam}(\rho_2)$ and $\rho_2^{jam}(\rho_1)$ are the jam densities of vehicle class 1 and
 155 2, respectively. In this model, we adopt the speed function proposed in
 156 (Nair et al., 2011). This speed-density relationship is derived based on the
 157 assumption that the flow of vehicles is dictated by available free spaces along
 158 the way, and it is written as

$$v_i = v_i^f \left(1 - \int_0^{r_i^c} f(l(\rho_1, \rho_2)) dl \right), \quad (7)$$

159 where $f(l(\rho_1, \rho_2))$, v_i^f and r_i^c are, respectively, the probability density function
 160 (PDF) of the inter-vehicle spacing (pore), the free speed and the minimum
 161 traversable inter-vehicle space (critical pore size) of class i . As such, by
 162 relating the speed to the inter-vehicle spacing lane sharing, filtering and
 163 creeping behaviors of PTWs can be captured, rendering it more suitable for
 164 our purpose than any other multi-class speed functions. However, in (Nair
 165 et al., 2011) a closed form expression for the PDF of inter-vehicle spacing
 166 (pore) is missing. The same author later proposes exponential distribution
 167 (Nair et al., 2012) with intensity λ to characterize the inter-vehicle spacing,
 168 where λ is given as:

$$\lambda = (l_{max} - l_{min}) \left(1 - \sum_{i=1}^2 a_i \rho_i \right) + l_{min}.$$

169 This definition of the distribution parameter λ produces an incorrect result,
 170 i.e. the speed increases with increasing of vehicle class densities. Further-
 171 more, it does not describe the equilibrium speed uniquely for a given class

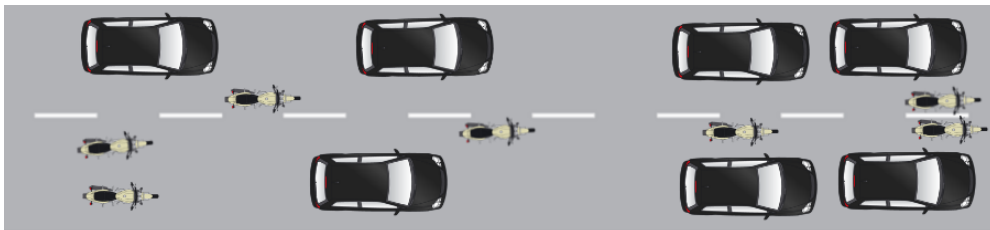


Figure 1: Heterogeneous traffic flow for PTWs and cars.

172 densities (the requirement defined in equation (6)). On the other hand, the
 173 exponential assumption is taken based on the longitudinal headway distri-
 174 bution. In order to fill this gap, we develop an analytical expression for the
 175 inter-vehicle spacing distribution based on simulation results. Further, we
 176 introduce an approximation method in order to determine the distribution
 177 parameters.

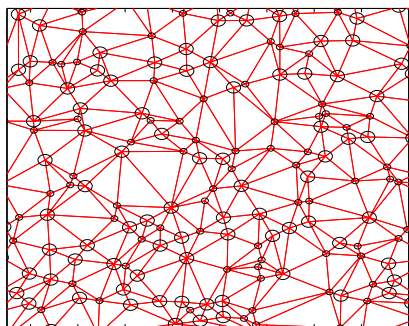
178 2.1. Vehicle spacing distribution

179 Vehicle-spacing distribution, which was referred as pore space distribu-
 180 tion, was first used to describe the speed-density relationship in the paper
 181 by Nair et al. (2011), yet the distribution was not known. Here, we pro-
 182 pose Poisson point process and Delaunay triangulation based method for the
 183 derivation of vehicle spacing distribution.

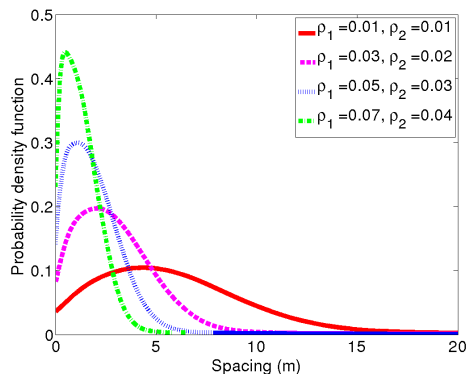
184 For the sake of simplicity, we take the following assumptions: cars and
 185 PWTs have a circular shape and they are distributed in the domain uniformly
 186 and independently according to Poisson point process with intensity λ , where
 187 λ is the number of vehicles per unit area. Although limited to non-dense
 188 traffic, the study done using real data in (Jiang et al., 2016) supports the
 189 Poisson point process assumption for the spatial distribution of vehicles on
 190 the road. The circular shape of vehicles that is introduced for simplification
 191 does not change the distribution of the inter-vehicle spacing qualitatively.
 192 Furthermore, Delaunay triangulation is used to define the spacing between
 193 vehicles on the assumption that Delaunay triangle edge length represents the
 194 size of the spacing.

195 Given the density of each vehicle classes, vehicles are placed uniformly
 196 and independently without overlapping in a two-dimensional finite space with
 197 intensity $\lambda = \rho_1 + \rho_2$. Here, ρ_1 and ρ_2 represent PTWs' and cars' areal
 198 density, i.e. vehicles per unit area, respectively. The Delaunay triangulation
 199 is constructed over the center of vehicles (Figure 2(a)) and the triangles edge

200 length data from multiple simulation runs is used to estimate the probability
 201 density function (Figure 2(b)).



(a) Delaunay triangulation over vehicles, one example scenario.



(b) Probability density function for different traffic compositions.

Figure 2: Vehicles spacing distribution, where ρ_1 and ρ_2 represent, respectively, PTWs and cars density

202 In (Miles, 1970) it is indicated that for a Delaunay triangulation per-
 203 formed on homogeneous planar Poisson point with intensity λ the mean
 204 value of the length of Delaunay triangle edge, and the square of the length
 205 are given by $E(l_p) = \frac{32}{9\pi\sqrt{\lambda}}$ and $E(l_p^2) = \frac{5}{\pi\lambda}$, respectively. We then convert
 206 these formulations to our problem where we have circles, instead of points.
 207 When the points are replaced by circles (small circles for PTWs and large
 208 circles for cars), edge length measured for points is reduced by the sum of
 209 the radius of the circles the two end points of the edge. For instance, an edge
 210 connecting PTWs and cars is reduced by $R_1 + R_2$, where R_1 and R_2 are the
 211 radius of a circle representing the PTW and the car respectively.

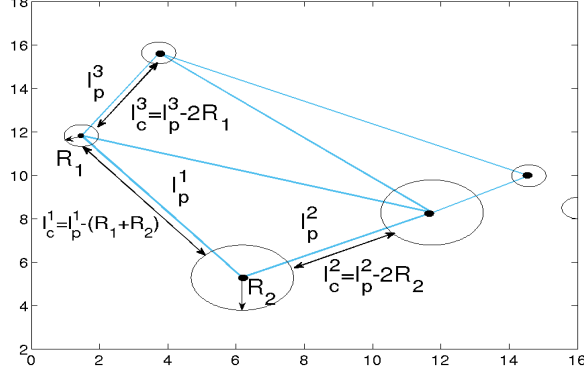


Figure 3: Delaunay triangle edges length for circles.

212 In accordance with the mean length of the delaunay traingle edge over
 213 points, we define for circles as (Figure 3):

$$E[l_c] = E[l_p] - 2(R_1 p_1 + R_2 p_2),$$

214 where p_1 is probability for an edge to touch PTWs and p_2 for cars. This
 215 probability is expressed in the form $p_i = \frac{\rho_i}{\rho_1 + \rho_2}$, therefore we get

$$E(l_c) = \mu = \frac{32}{9\pi\sqrt{\rho_1 + \rho_2}} - \frac{2(R_1\rho_1 + R_2\rho_2)}{\rho_1 + \rho_2}.$$

216 Standard deviation and variance are the same for the case of points (σ_p^2) and
 217 circles(σ_c^2), thus

$$\sigma_p^2 = E(L_p^2) - E(L_p)^2 \approx \frac{3}{\pi^2\lambda}, \quad \sigma_c^2 = \frac{3}{\pi^2(\rho_1 + \rho_2)}.$$

218 The above equations provide the parameters for the distribution function of
 219 inter vehicle-spacing, we then identify the best fitting theoretical distribution.
 220 To determine a theoretical probability density function (PDF) that best fits
 221 the observed PDF, we use MATLAB's curve fitting tool, and the goodness of
 222 the fit is measured by R-square, sum of squared errors (SSE) and root mean
 223 square error (RMSE) values. We consider left-truncated normal, log-normal

224 and exponential as candidate distributions to characterize vehicle-spacing.
 225 The distributions are chosen based on qualitatively observed similarity on
 226 the shape of PDF curve. We also include the exponential distribution, which
 227 is recommended in (Nair et al., 2012). The comparison between the three
 228 selected theoretical distribution functions is shown in Figure 4. Based on the
 229 goodness of the fit results, see Table 1, left-truncated normal (LT-Normal)
 230 distribution conforms better to the estimated PDF than the other distribu-
 231 tions. Besides, it can be noted that the negative exponential assumption
 232 taken in (Nair et al., 2012) is not fitting well.

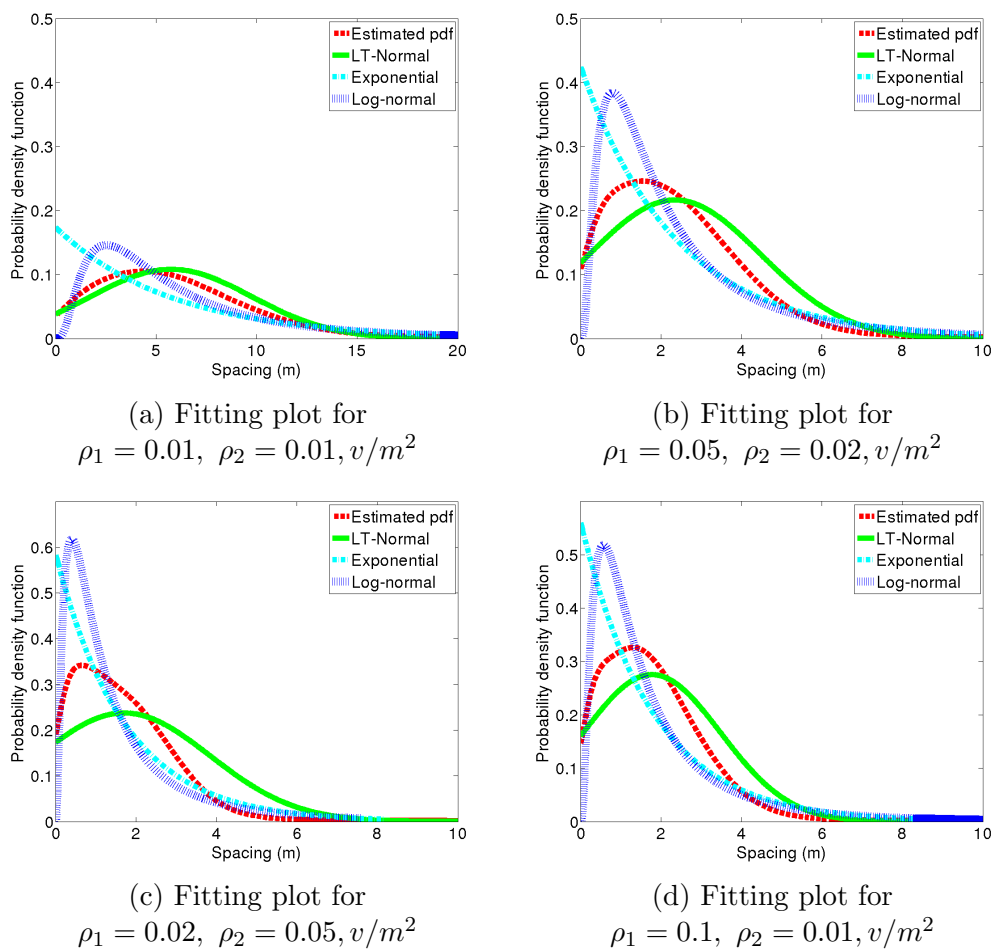


Figure 4: Comparison of estimated probability distribution function and fitting theoretical distributions for different vehicles composition

	SSE	R-square	RMSE	SSE	R-square	RMSE
	$\rho_1 = 0.01, \rho_2 = 0.01$			$\rho_1 = 0.05, \rho_2 = 0.02$		
LT-normal	0.24	0.955	0.0069	0.97	0.938	0.0139
Log-normal	0.809	0.851	0.0127	2.67	0.831	0.023
Exponential	2.17	0.602	0.0208	4.05	0.744	0.028
	$\rho_1 = 0.02, \rho_2 = 0.05$			$\rho_1 = 0.1, \rho_2 = 0.01$		
LT-normal	3.21	0.853	0.025	1.46	0.993	0.017
Log-normal	5.51	0.748	0.033	4.07	0.813	0.028
Exponential	3.93	0.82	0.028	5.39	0.753	0.032

Table 1: Goodness of the fit measures obtained from the fitting experiments for different theoretical distributions.

233 We added minimum distance rejection criteria (minimum allowable dis-
234 tance) to Poisson point process distribution so that vehicles do not overlap,
235 resulting in change of inter vehicle spacing distribution property (E.g. the
236 average, variance...of the distribution). Due to this, we observed that the
237 road width and ratio of vehicle classes have an influence on the PDF. The
238 effect of the size of the area is pronounced when $L \gg W$, where L and W
239 denote length and width of the area (see Figure 5). The significance of the
240 variation also depends on the ratio of the two densities. Yet, left-truncated
241 normal distribution remains the best fit and gives a good approximation in
242 most of the situation.

243 Therefore, we assume that the spacing distribution follows the left-truncated
244 normal distribution, having the form

$$f_{pTN}(l) = \begin{cases} 0 & l < 0 \\ \frac{f_p(l)}{\int_0^\infty f_p(l)} & l \geq 0 \end{cases} \quad \text{where } f_p = \frac{1}{\sqrt{2\pi}\sigma} \exp \frac{-(x - \mu)^2}{2\sigma^2}. \quad (8)$$

245 2.2. Speed-density relationship

246 Using the PDF function in equation (8), the speed-density relationship
247 in equation (7) is re-written as

$$v_i = v_i^f \left(1 - \int_0^{r_i^c} f_{pTN}(l) dl \right), \quad (9)$$

248 where v_i^f and r_i^c represent the free flow speed and the critical pore size,
249 respectively, of class i. The critical pore size depends on the traffic situation

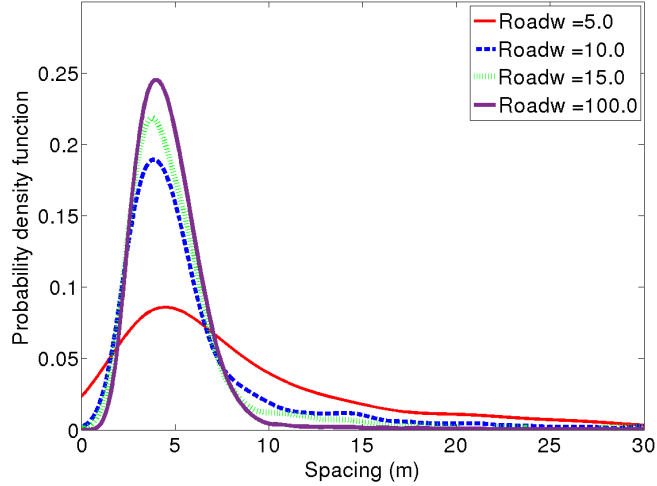


Figure 5: Example $\rho_1 = \rho_2 = 0.03 \text{ veh}/m^2$: PDF of the inter-vehicle distance on a road with dimension $L = 100$ and W ranging from $5m - 100m$

250 and the interacting vehicle class (Ambarwati et al., 2014). The critical pore
 251 size accepted by vehicles when travelling at higher speed is larger than the
 252 critical pore size at lower speeds. To reproduce the critical pore size - speed
 253 proportionality (Minh et al., 2012), for example, we can formulate the critical
 254 pore size as:

$$r_c = r_c^{min} + r * (1 - (\rho_1 * A_1 + \rho_2 * A_2)),$$

255 where $\rho_1, A_1, \rho_2, A_2, r_c^{min}$ and r denote density of PTW, area of PTW, density
 256 of car, area of car, the minimum critical pore size, and the difference between
 257 the maximum and the minimum critical pore size, respectively. As such, the
 258 critical pore size increases with increasing speed or with decreasing vehicle
 259 class densities, which is in agreement with the gap acceptance theory. To
 260 evaluate the impact of the critical pore on the speed function, we compare
 261 the result for a constant critical pore size and a critical pore size scaled
 262 according to the actual traffic. As depicted in Figure 6, the critical pore size
 263 doesn't change the qualitative behavior of our fundamental diagram. Since
 264 the critical pore size does not have any qualitative implication, for simplicity
 265 we use a constant value. The limitation of equation (9) is that, because of
 266 the property of normal distribution function, the speed becomes zero only
 267 at infinite density, as for the speed function used in (Nair et al., 2011). In
 268 attempt to overcome this infinite jam density, we have distinguished the jam

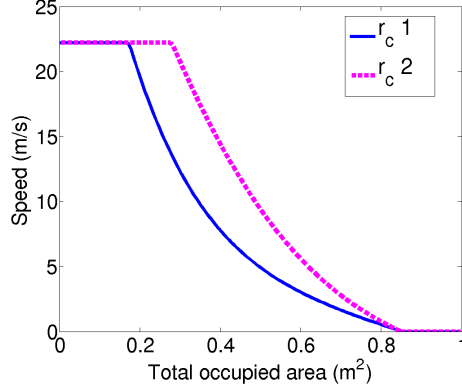


Figure 6: Speed vs total occupied area for constant critical pore size ($r_c^2 = 3m$) and a variable critical pore size (r_c^1) with the following parameters $r_c^{min} = 3m$ and $r = 2m$.

269 area occupancy for the two classes, and the speed values are normalized to
 270 zero at the jam area occupancy. Beside the consideration of vehicles size,
 271 we selected the jam area occupancies for the two classes in such a way to
 272 allow filtering of PTWs through completely stopped cars traffic (Fan and
 273 Work, 2015). We distinguish the maximum total occupied area, which is the
 274 extreme total occupied areas corresponding to the null speed of a vehicle
 275 class, for the two classes in such a way that

$$V_2(A_{max}^2) = 0, V_1(A_{max}^2) > 0, V_2(A_{max}^1) = V_1(A_{max}^1) = 0, A_{max}^2 < A_{max}^1 \quad (10)$$

276 where V_2, V_1, A_{max}^2 and A_{max}^1 represent the speed of cars, the speed of PTWs,
 277 the maximum total occupied area of cars and the maximum total occupied
 278 area of PTWs, respectively. Accordingly, when the total area occupied by
 279 vehicles equals A_{max}^2 , the cars completely stop while the average speed of
 280 PTWs is greater than zero. Due to this, PTWs can move through jammed
 281 car until the total area occupied by vehicles reaches to A_{max}^1 . On the grounds
 282 of the relation in eqn. (10) and some realistic conditions, we approximate
 283 the jam area occupancy, i.e. $\rho_1 A_1 + \rho_2 A_2$, to 1 for PTWs and to 0.85 for
 284 cars, where ρ, A stand for density (veh/m^2) and projected area of vehicles
 285 (m^2), respectively.

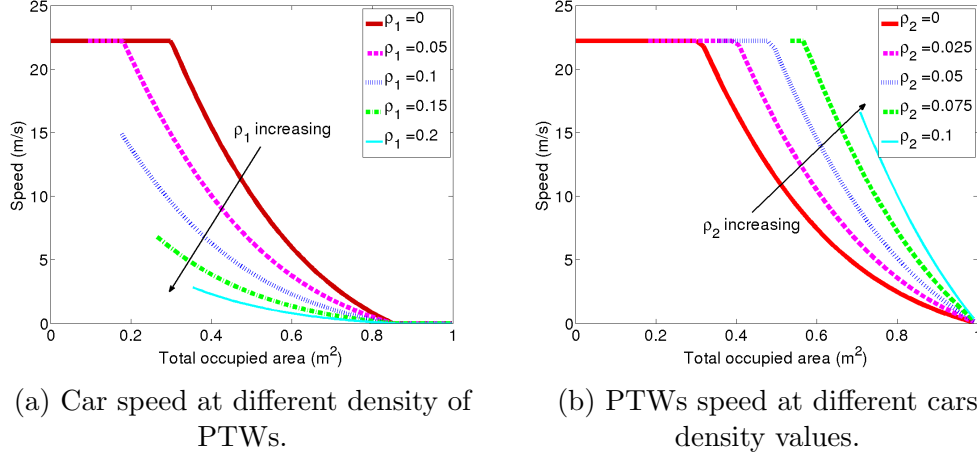


Figure 7: Speed Vs total occupied area ($\sum \rho_1 A_1 + \sum \rho_2 A_2$), where $\rho_1 A_1$ and $\rho_2 A_2$ are area projected on the road by PTW and car, respectively.

286 Further modification is applied to the speed function in order to comply
 287 with triangular fundamental diagram theory, that is presence of two regimes,
 288 specifically, congestion and free flow regime (Newell, 1993). In free flow there
 289 is no significant drop of average speed with the increase of density. However,
 290 beyond some critical density value, the average speed of vehicles decreases
 291 with density increase. Therefore, we adjust the speed functions to:

$$v_1 = \min \left\{ v_1^f, C_v v_1^f \left(1 - \frac{1}{N_1} \int_0^{r_1^c} f_{PTN}(l) dl \right) \right\}, \quad (11)$$

292

$$v_2 = \min \left\{ v_c^f, C_v v_2^f \left(1 - \frac{1}{N_2} \int_0^{r_2^c} f_{PTN}(l) dl \right) \right\}, \quad (12)$$

293 where N_i is a speed normalization factor and C_v is a scaling factor so that
 294 v_i equals the free flow speed at critical density in the presence of traffic of
 295 vehicle class i only. After all the modifications, the speed-density relation
 296 look as shown in Figure 7. Different from the existing models which describe
 297 traffic composition in terms of total area/space occupancy (Nair et al., 2012)
 298 (Fan and Work, 2015)(Benzoni-Gavage and Colombo, 2003), one of the key
 299 characteristics of our speed model is that it captures well the variation in
 300 traffic composition as the speed is expressed as a function of the density of
 301 each vehicle class. Specifically, for a given area occupancy, depending on the
 302 proportion of one class of vehicles the speed value varies. For instance, for a

303 given area occupancy, the higher the percentage of PTWs the higher becomes
 304 the number of vehicles and the average pore size shrinks. In turn, the speed
 305 value decreases. The general properties of our speed model are summarized
 306 as follows:

- 307 1. A unique speed value is associated with a given total density and traffic
 308 composition.
- 309 2. In free flow, vehicles move at constant (maximal) speed.
- 310 3. In congestion, speed decreases with increase of density.
- 311 4. Speed depends on the densities of the two vehicle classes and their
 312 proportion.
- 313 5. For the same occupancy area (total area occupied by vehicles) the more
 314 the share of PTWs is the lower becomes the speed, which is the main
 315 property missed by multi-class models that define the speed function
 316 in terms of area occupancy.
- 317 6. Each class has a different fundamental relation
- 318 7. Each class has a distinctive critical and jam densities parameters.

319 None of the models known to us satisfies all the aforementioned properties,
 320 although there are models that satisfy a few of them. Property (3), (4) and
 321 (6) are common to most of multi-class LWR models. Nonetheless, models
 322 that describe speed as a function of total occupied space (Benzoni-Gavage
 323 and Colombo, 2003; Fan and Work, 2015; Chanut and Buisson, 2003) do not
 324 satisfy property (1). While (Van Lint et al., 2008) satisfies property (1) and
 325 (Fan and Work, 2015) satisfies property (7), property (5) is unique to our
 326 model.

327 *2.3. Model Analysis*

328 To describe the solution of the system equations (3)-(5) in terms of wave
 329 motion, the jacobian matrix Dq of $q = (q_1, q_2)$ should be diagonalizable with
 330 real eigenvalues, in another word the system has to be hyperbolic. We can
 331 prove the hyperbolicity by showing that the system is symmetrizable, i.e.
 332 there exists a positive-definite matrix S such that SDq is symmetric, see
 333 (Benzoni-Gavage and Colombo, 2003).

334 Re-writing the system in the form:

$$\frac{\partial \rho}{\partial t} + Dq(\rho) \frac{\partial \rho}{\partial x} = 0,$$

335 where

$$\rho = \begin{bmatrix} \rho_1 \\ \rho_2 \end{bmatrix} \quad \text{and} \quad q(\rho) = \begin{bmatrix} \rho_1 v_1(\rho) \\ \rho_2 v_2(\rho) \end{bmatrix},$$

336 the Jacobian matrix of $q(\rho)$ is given by:

$$Dq(\rho) = \begin{bmatrix} \frac{\partial(\rho_1 v_1)}{\partial \rho_1} & \frac{\partial(\rho_1 v_1)}{\partial \rho_2} \\ \frac{\partial(\rho_2 v_2)}{\partial \rho_2} & \frac{\partial(\rho_2 v_2)}{\partial \rho_1} \end{bmatrix} = \begin{bmatrix} \rho_1 \partial_1(v_1) + v_1 & \rho_1 \partial_2(v_1) \\ \rho_2 \partial_1(v_2) & \rho_2 \partial_2(v_2) + v_2 \end{bmatrix}$$

337 For $\rho_1 > 0, \rho_2 > 0$,

$$S = \begin{bmatrix} \frac{1}{\rho_1 \partial_2(v_1)} & 0 \\ 0 & \frac{1}{\rho_2 \partial_1(v_2)} \end{bmatrix} \quad (13)$$

338 is a symmetrizer of Dq , thus the system satisfies the hyperbolicity condition.

339

340 The eigenvalues of the Jacobian representing information propagation
341 (characteristic) speed are given by:

$$\lambda_{1,2} = \frac{1}{2} \left[\alpha_1 + \alpha_2 \pm \sqrt{(\alpha_1 - \alpha_2)^2 + 4\rho_1 \rho_2 \partial_2(v_1) \partial_1(v_2)} \right],$$

342 where

$$\alpha_1 = \rho_1 \partial_1(v_1) + v_1, \quad \alpha_2 = \rho_2 \partial_2(v_2) + v_2.$$

343 Following (Benzoni-Gavage and Colombo, 2003, Proposition 3.1) it is possible
344 to show that

$$\lambda_1 \leq \min\{\alpha_1, \alpha_2\} \leq \min\{v_1, v_2\} \text{ and } \min\{v_1, v_2\} \leq \lambda_2 \leq \max\{v_1, v_2\}, \quad (14)$$

345 where, we have taken $\lambda_1 \leq \lambda_2$. The proof in (Benzoni-Gavage and Colombo,
346 2003) assumes that $V_1 > V_2$ to exclude the degenerate case, when $V_1 =$
347 V_2 . However, Zhang et al. (Zhang et al., 2006) also studied the prop-
348 erties of a similar model as in (Benzoni-Gavage and Colombo, 2003), but
349 here for a generic speed function which is expressed as a function of total
350 density, i.e. $v_i = v_i(\rho)$, where $\rho = \sum_i \rho_i$. Accordingly, it is proved
351 that for $v_1 < v_2 < v_3 \dots < v_m$, the eigenvalues are bounded such that
352 $\lambda_1 < v_1 < \lambda_2 < v_2 < \lambda_3 < \dots < v_m - 1 < \lambda_m < v_m$ (refer (Zhang et al.,
353 2006, Theorem 3.1, Lemma 2.2, Lemma 2.3)). Due to the complexity of the
354 dependency of the speed function on vehicle class densities, we could not fol-
355 low a similar analytical approach. Nonetheless, we have checked the validity

356 of this relationship, i.e. $\lambda_1 < v_1 < \lambda_2 < v_3 < \lambda_3 < \dots v_m - 1 < \lambda_m < v_m$,
 357 using a graphical analysis, by taking a specific case where $v_1 > v_2$ is not true
 358 in all traffic states. In our model, $v_1 > v_2$ is not always satisfied when the
 359 maximum speed of cars is higher than PTWs'. Hence, for the test, the maximum
 360 speed of cars is set to be greater than the maximum speed of PTWs.
 361 Let $\lambda_1 = \min \{\lambda_1, \lambda_2\}$ and $\lambda_2 = \max \{\lambda_1, \lambda_2\}$, if the relation $\lambda_1 < \min \{v_1, v_2\} <$
 362 $\lambda_2 < \max \{v_1, v_2\}$ holds, then $\max \{v_1, v_2\} - \lambda_2 > 0$, $\min \{v_1, v_2\} - \lambda_2 < 0$ and
 363 $\min \{v_1, v_2\} - \lambda_1 > 0$. Figure 8(a) shows that $\max(v_1, v_2) - \lambda_2 > 0$, implying
 364 $\lambda_2 < \max(v_1, v_2)$. From Figure 8(b) it can be learned that $\min(v_1, v_2) - \lambda_2 <$
 365 0 , thus $\min(v_1, v_2) < \lambda_2$. Figure 9 shows that $\min(v_1, v_2) - \lambda_1 > 0$ over all
 point in $S = \{\rho_1, \rho_2\}$, thus $\lambda_1 < \min(v_1, v_2)$.

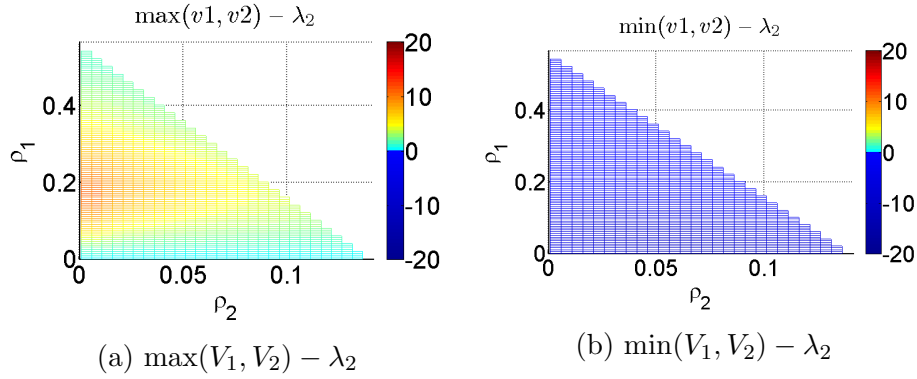
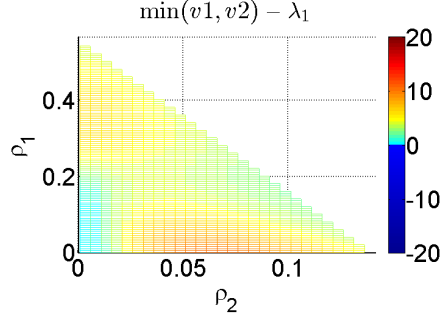


Figure 8: Evaluation of the maximum characteristics speed over a point in $S = \{\rho_1, \rho_2\}$,
 Here $V_1 = 22m/s$ and $V_2 = 27m/s$

366



(a) $\min(V_1, V_2) - \lambda_1$

Figure 9: Evaluation of minimum characteristics speed over a point in $S = \{\rho_1, \rho_2\}$, Here $V_1 = 22m/s$ and $V_2 = 27m/s$

367 The results from the graphical analysis strongly suggest that the relation
 368 in equation (14) is valid for our model, which confirms that in the model no
 369 wave travels at a higher speed than the traffic and thus the wave propagation
 370 speed is finite.

371 2.4. Model discretization

372 To simulate the traffic flow we need the solution of the traffic equation
 373 in Eq. (3). Thus, we apply a conservative finite volume method for the
 374 approximation of the numerical solution. In the approximation, the spatial
 375 domain is divided into equal grid cells of size Δx and at each time interval
 376 Δt the density value in the domain is updated according to the conservation
 377 law. Rewriting in the integral form it becomes

$$\frac{d}{dt} \int_{x_{i-1/2}}^{x_{i+1/2}} \rho(x, t) dx = q(\rho(x_{i-1/2}, t)) - q(\rho(x_{i+1/2}, t)) \quad (15)$$

Integrating eq. (15) in time from t^n to $t^{n+1} = t^n + \Delta t$, we have

$$\begin{aligned} \int_{x_{i-1/2}}^{x_{i+1/2}} \rho(x, t^{n+1}) dx &= \int_{x_{i-1/2}}^{x_{i+1/2}} \rho(x, t^n) dx \\ &+ \int_{t^n}^{t^{n+1}} q(\rho(x_{i-1/2}, t)) dt - \int_{t^n}^{t^{n+1}} q(\rho(x_{i+1/2}, t)) dt. \end{aligned} \quad (16)$$

378 After some rearrangement of Eq. (16), we obtain an equation that relates
 379 cell average density ρ_j^n update with average flux values at the cell interfaces.

$$\rho_i^{n+1} = \rho_i^n - \frac{\Delta t}{\Delta x} [F_{i+1/2}^n - F_{i-1/2}^n], \quad (17)$$

380 where $F_{i+1/2}^n$ is an average flux value at the cell interface $x = x_{i+1/2}$:

$$F_{i+1/2}^n = \mathcal{F}(\rho_i^n, \rho_{i+1}^n), \quad \text{where } \mathcal{F} \text{ is the numerical flux function.} \quad (18)$$

381 Accordingly, equation (17) rewrites

$$\rho_i^{n+1} = \rho_i^n - \frac{\Delta t}{\Delta x} [\mathcal{F}(\rho_i^n, \rho_{i+1}^n) - \mathcal{F}(\rho_{i-1}^n, \rho_i^n)]. \quad (19)$$

382 In the absence of a general Riemann solver, numerical methods for multi-class
 383 LWR model based on a generalization of the cell transmission model (CTM)
 384 supply and demand functions for each vehicle class have been introduced
 385 in (van Wageningen-Kessels, 2013; Fan and Work, 2015). However, these
 386 algorithms are computationally expensive to implement in our case, due to
 387 the lack of analytical expression for computing the numerical flux. Therefore,
 388 we have opted for the Lax-Friedrichs scheme (LeVeque, 1992), which is easier
 389 to implement and gives a good accuracy at sufficiently refined meshes. The
 390 numerical flux function is therefore given by

$$\mathcal{F}(\rho_i, \rho_{i+1}) = \frac{1}{2}(q(\rho_i) + q(\rho_{i+1})) + \frac{\alpha}{2}(\rho_i - \rho_{i+1}), \quad (20)$$

391 where α is the numerical viscosity satisfying the condition $\alpha \geq V_{max} =$
 392 $\max\{v_1^f, v_2^f\}$. The space and time steps Δx and Δt are selected to meet
 393 Courant, Friedrichs and Lewy (CFL) condition, which is a necessary condi-
 394 tion for a numerical method to achieve stability and convergence. Therefore,
 395 Δt is chosen to satisfy $\Delta t \leq \Delta x/V_{max}$, due to the bounds on the eigenvalues
 396 derived in Section 2.3.

397 3. Model Verification

398 The verification experiments are intended to evaluate our proposed model
 399 against the baseline model in (Nair et al., 2011), and the required qualitative
 400 behaviors.

401 *3.1. Pore size distribution verification*

402 Here, we verify the pore size distribution against the results in (Nair
 403 et al., 2011), which are produced by determining the cumulative distribution
 404 of the pore size from the average of multiple simulation outcomes. We ex-
 405 pect that the vehicle spacing distribution we propose yields qualitatively the
 406 same result as multiple simulation runs. To derive the pore size distribution,
 407 we have introduced simplification assumptions which are not used in (Nair
 408 et al., 2011). The impact of these assumptions on the model behavior can
 409 be grasped through the qualitative comparison between the results from our
 410 model and (Nair et al., 2011).

411 Therefore, we reproduce the result in (Nair et al., 2011) following the same
 412 approach used in the paper. In Nair’s approach, for each configuration, the
 413 fraction of accessible pores is determined by running multiple simulation run,
 414 where vehicles are randomly placed in the domain (without overlapping) and
 415 then the probability of finding a pore greater than the critical pore size is
 416 determined from this configuration. However, at high density it may not be
 417 possible to find a solution within a reasonable amount of time. In these cases,
 418 the author proposed to adjust the pore space distribution to reflect ‘unplaced
 419 vehicles’. But, nothing is mentioned in the paper how the pore space distri-
 420 bution can be adjusted. Thus, we applied our own method for adjusting the
 421 pore size distribution. For a given total number of vehicles, first the fraction
 422 of accessible pore (F_c) is determined according to the ‘placed vehicles’. If all
 423 the vehicles can not be placed within the time limit set, F_c will be reduced
 424 by a ratio of total number of ‘placed vehicles’ to total number of vehicles.

425 For the sake of comparison, we use similar loading profile and simulation
 426 parameters. With *normal profile*, the interaction of the two classes under
 427 uninterrupted flow conditions is studied, while a traffic flow with disruption
 428 is studied in *queue profile*. The maximum speed is set to $V_1 = 80km/hr$ for
 429 PTWs and $V_2 = 100Km/hr$ for cars. The simulation is done for 300s on
 430 the space domain $x \in [0, 3000m]$, and with homogeneous initial density of
 431 $\rho_1(x, 0) = 0, \rho_2(x, 0) = 0$. We also set $\Delta x = 100m$ and $\Delta t = 2.5sec$. For
 432 both experiments the upstream inflow is set to:

433

$$F_1(0, t) = \begin{cases} 0.5veh/sec & \text{for } t \in [100s, 200s], \\ 0 & \text{otherwise,} \end{cases}$$

434

$$F_2(0, t) = \begin{cases} 0.5 \text{ veh/sec} & \text{for } x \in [0s, 200s], \\ 0 & \text{otherwise,} \end{cases}$$

435

436 and we give absorbing boundary conditions downstream, so that the vehicles
 437 leave freely.

438 From Figure 10, it can be observed that PTWs traffic density wave moves
 439 faster than cars. Due to this, although PTWs starts behind, they move past
 440 cars traffic and leave the simulation domain faster. At $t = 250\text{sec}$, all PTWs
 441 have overtaken cars. Both models behave similarly except small quantitative
 changes.

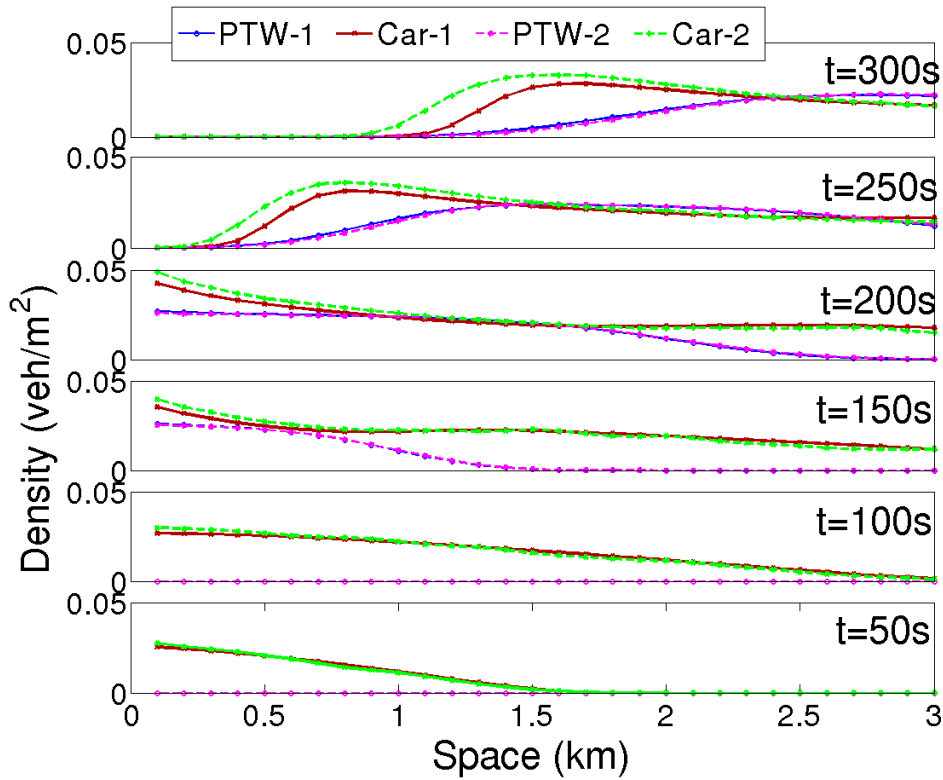


Figure 10: *Normal profile*, traffic density waves of cars and PTWs at different time steps. (PTW-1, Car-1) and (PTW-2, Car-2) represent result form our model and Nair’s model, respectively.

442

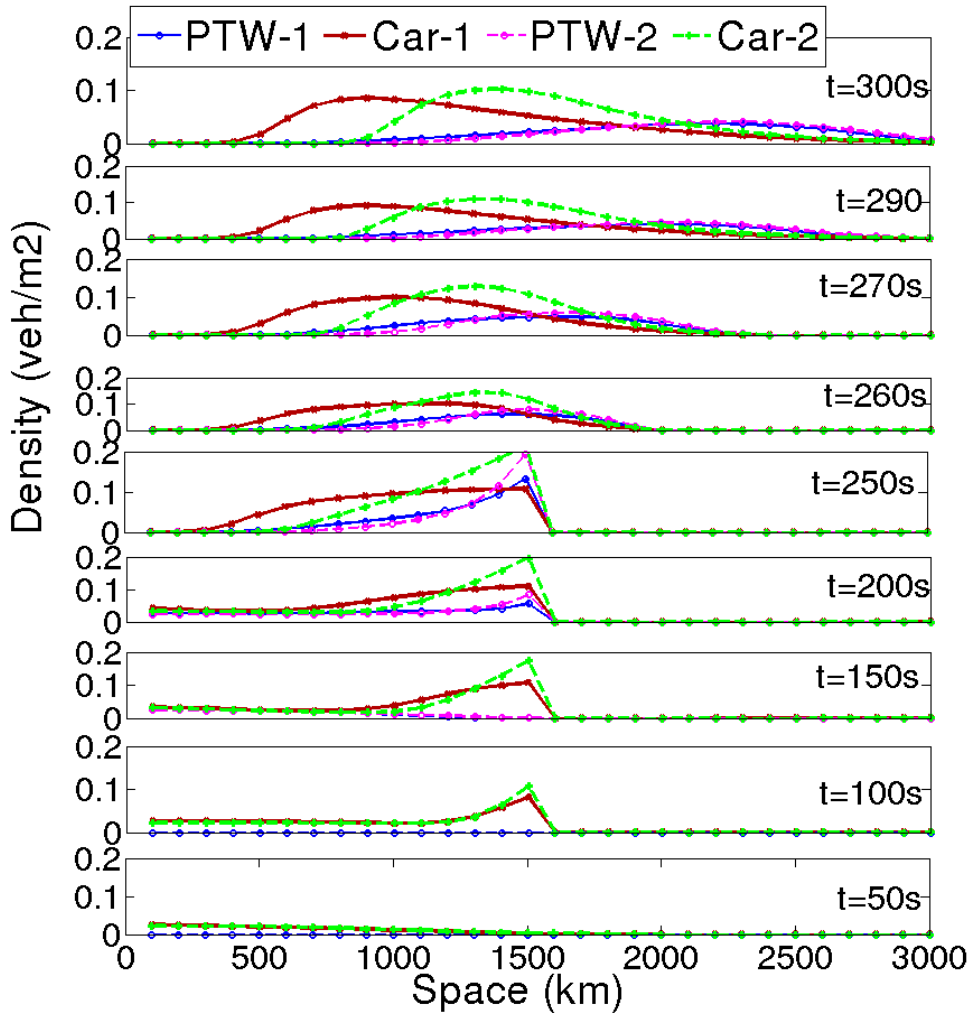
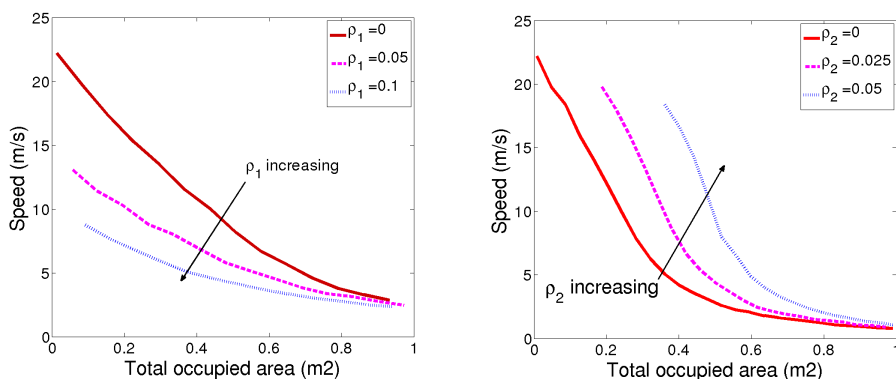


Figure 11: *Queue profile*, traffic density waves of cars and PTWs at different time steps. (PTW-1, Car-1) and (PTW-2, Car-2) represent result form our model and Nair’s model, respectively.

443 The result in Figure 11 represents the interrupted scenario, where for
 444 $t \in [0sec, 250sec]$ the flow is blocked at the mid of roadway (at 1500m). Im-
 445 portant properties observed from the results are: PTWs are able to move to
 446 the front of the queue passing stationary cars (from $t = 200sec$ to $t = 250sec$),
 447 thus, when the blockage is removed, PTWs clear first. In this scenario, a
 448 big quantitative divergence is observed between the two models, particularly

449 when the queue is formed. In our model, we defined jam densities for each
 450 class and the speed function is scaled to reach zero at the jam densities
 451 (section 2.1, Figure 7). But, this modification is not applied to the speed
 452 function in Nair’s model, see Figure 12. The difference between the speed
 453 values becomes more significant at the higher densities. The resulting quan-
 454 titative change mainly happens because of the speed difference. Otherwise,
 455 both models are quantitatively similar.
 456 The results in Figures 10 and 11, have almost the same qualitative properties
 457 as the results in (Nair et al., 2011), confirming the validity of the assumptions
 made to establish the distribution function of inter-vehicle spacing.



(a) Car speed at different density of PTWs (b) PTWs speed at different cars density values.

Figure 12: Speed Vs total occupied area ($\sum \rho_1 A_1 + \sum \rho_2 A_2$) Nair’s model (Nair et al., 2011), where $\rho_1 A_1$ and $\rho_2 A_2$ are area projected on the road by PTW and car, respectively.

458

459 3.2. Verifying model properties

460 In this section, the capability of our model to reproduce the observed
 461 macroscopic phenomena of mixed flow of PTWs and cars is evaluated. The
 462 following two well-known features (Fan and Work, 2015) are used as a bench-
 463 mark to evaluate our model.

- 464 • **Overtaking-** when the traffic volume is high, cars start slowing down.
 465 However, PTWs remain unaffected or less affected by the change in
 466 traffic situation, as they can ride between traffic lanes. As a conse-
 467 quence, PTWs travel at higher speed and overtake slow moving cars.

468 • **Creeping**- when cars are stopped at traffic signals or because of traffic
 469 jams, PTWs can find a space to filter (creep) through stationary cars
 470 and move ahead.

471 In addition, a comparison with the models in (Benzoni-Gavage and Colombo,
 472 2003) and (Fan and Work, 2015), hereafter referred as *N-pop* and *creeping*
 473 respectively, is presented along with the verification of our model, *porous G*.

474 For creeping and overtaking experiments, the parameters in Table 2 are
 chosen. Jam density refers to the maximum area occupancy, which equals to

	PTW	Car
Vehicle length (m)	1.5	3
Vehicle radius (m)	0.75	1.5
Max. speed (m/s)	1.8	1
Jam density <i>porous G</i>	1	0.85
Jam density <i>creeping</i>	1.8	1
Jam density <i>N-pop</i>	1	1

Table 2: Simulation Parameters

475
 476 $\rho_1 A_1 + \rho_2 A_2$ for *porous G* model and $\rho_1 l_1 + \rho_2 l_2$ for the other models, where
 477 vehicles come to complete stop state. The simulation is done on a road of
 478 length $50m$ and $\Delta x = 0.05m$ and Δt is selected according to CFL condition.

479 3.2.1. Creeping experiment

480 A signalized intersection is employed for testing creeping. In the simula-
 481 tion, PTWs start behind the cars traffic and cars traffic have concentrated
 482 close to the traffic signal, so that PTWs arrive after most of the cars reached
 483 a complete stop. The simulation is done for $200sec$ and starts with initial
 484 densities

$$485 \rho_1(x, 0) = \begin{cases} 0.25 & \text{for } x \in [1m, 21m], \\ 0 & \text{otherwise,} \end{cases} \quad \rho_2(x, 0) = \begin{cases} 0.25 & \text{for } x \in [31m, 50m], \\ 0 & \text{otherwise.} \end{cases}$$

488 The inflow and outflow at the boundaries are set to zero. At the time PTWs
 489 start catching up cars traffic (Figure 13(a)), most of the cars are at stationary
 490 state (see Figure 13(a) lower subplot space location $45 - 50m$). However, as
 491 shown in Figure 13(b), PTWs maneuver through those stationary cars and

492 reach the front of the queue for the case of *creeping* and *Porous G* mod-
 493 els. For the *N-pop* model, the PTWs traffic stays behind the cars since both
 494 classes have the same jam density. Table 3 shows the average speeds of PTWs
 495 and cars in a particular location at time $t = 50s$. As can be observed from
 496 the speed values, unlike *N-pop* model, in the other two models PTWs have
 a non-zero speed value even though cars are at a complete stop state.

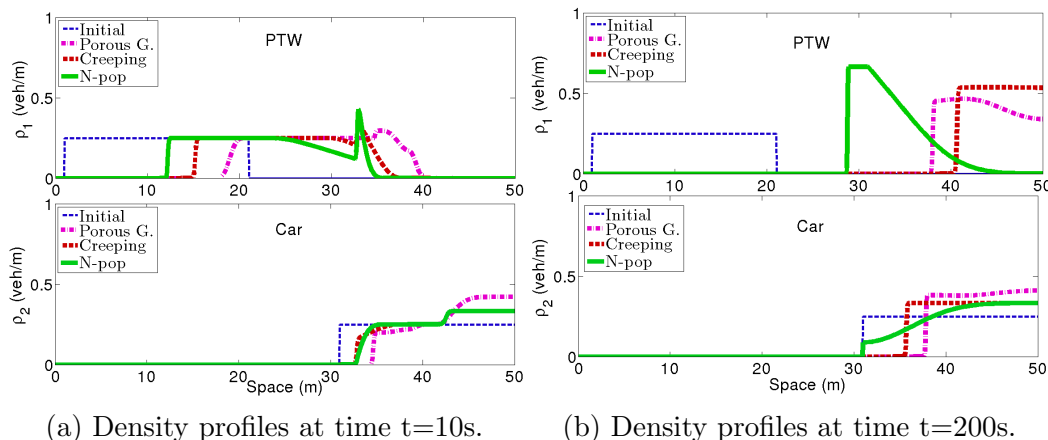


Figure 13: Creeping experiment density-space diagram, upper subplot for PTWs and lower subplot for cars.

497

	<i>Creeping</i>	<i>Porous G</i>	<i>N-pop</i>
V_1	0.2179	0.6349	0
V_2	0	0	0

Table 3: Speed values extracted at time $t = 50sec$ and position $x = 39.15m$

498 The results from the creeping experiment show similar behavior to the
 499 situation we may observe in real scenarios, i.e. PTWs seep through cars
 500 queue to reach the head the queue, both for *Porous G* and *Creeping* models.
 501 However, for the *N-pop* model, PTWs remain behind car traffic queue. Thus,
 502 only the first two models are able to produce this predominantly observed
 503 phenomenon of mixed traffic flow of cars and PTWs.

504 3.2.2. Overtaking experiment

505 For the overtaking scenario, car traffic is placed ahead of PTWs. The
 506 simulation starts with the initial state where:

507

$$508 \quad \rho_1(x, 0) = \begin{cases} 0.3 & \text{for } x \in [1m, 20m], \\ 0 & \text{otherwise,} \end{cases} \quad \rho_2(x, 0) = \begin{cases} 0.3 & \text{for } x \in [15m, 34m], \\ 0 & \text{otherwise.} \end{cases}$$

509

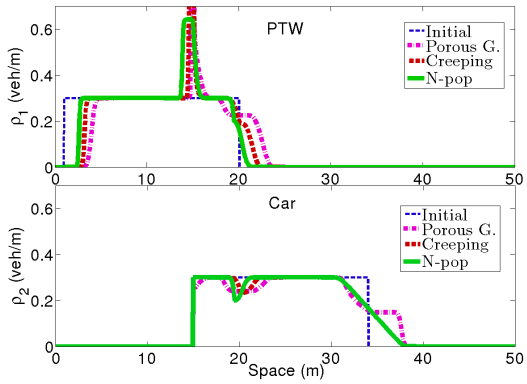
510 The inflow at the upstream boundary is set to zero and vehicles are al-
 511 lowed to leave freely at the downstream boundary. For this experiment, we
 512 consider two cases one when free flow speed of PTWs is higher than cars
 513 and the other when cars take the higher free flow speed. The occurrence of
 514 overtaking is evaluated by inspecting the evolution of traffic densities of the
 515 two classes. Overtaking is said to happen when the density waves of the two
 516 classes come to the same level in space and one of the two go past the other,
 517 i.e the tail end of one class is before the other.

518 As Figure 14 depicts, when free flow speed of PTWs is greater than cars,
 519 PTWs overtake cars in all the three models. In *Porous G* model overtaking
 520 is observed around at time $t = 18sec$ (Figure 14(b)), and for *Creeping* and
 521 *N-pop* models overtaking happens at $t = 38sec$ (Figure 14(c)) and $t = 80sec$
 522 (Figure 14(d)), respectively.

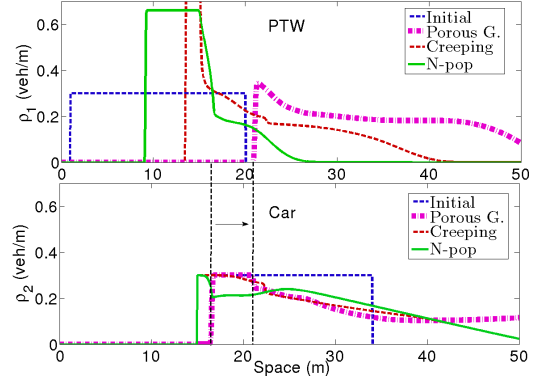
523 The simulation results in Figure 15 correspond to the case where free flow
 524 speed of cars ($V_2 = 1.8$) is greater than free flow speed of PTWs ($V_1 = 1.5$).
 525 As shown, in the two models, *Porous G* and *Creeping*, overtaking is observed.
 526 In *Porous G* model overtaking happens around time $t = 26sec$ (Figure 15(b))
 527 and at time $t = 40sec$ (Figure 15(c)) for *Creeping*. Nonetheless, *N-pop* model
 528 fails to reproduce overtaking. At time $t=52sec$ for *N-pop* the tail end of
 529 PTWs traffic is around location $x = 26m$ whereas for cars traffic it is around
 530 $x = 41m$ (Figure15(d)), which is far behind.

531 According to what is illustrated in Figures 14 and 15, all the three models
 532 are able to show the overtaking phenomenon when PTWs free flow speed is
 533 higher than cars. Further, for *Porous G* and *Creeping* models overtaking
 534 happens in the case where free flow speed of cars is higher than PTWs'
 535 as well. In *N-pop* model, unlike to the other two models, overtaking never
 536 happens unless car free flow speed is higher. This can be explained using a
 537 particular instance in Figure 16. As shown in the figure, in *Creeping* and
 538 *Porous G* models there exist a region where the speed of PTWs is greater
 539 than cars despite the free flow speed choice.

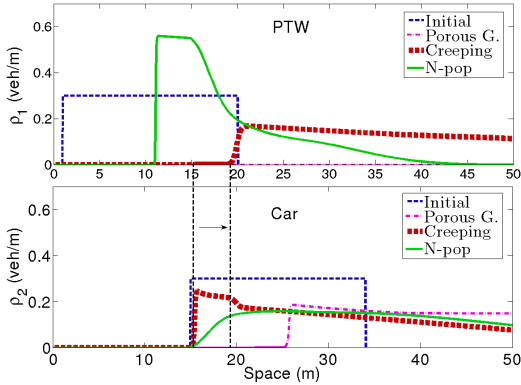
540 In conclusion, the model verification results validate that our model (*Porous*
 541 *G*) can reproduce the required creeping and overtaking phenomena. The *Creep-*
 542 *ing* model also satisfies all these properties. Yet, this model has a limitation,
 543 as occupied space is a mere factor that determines the speed and the varia-



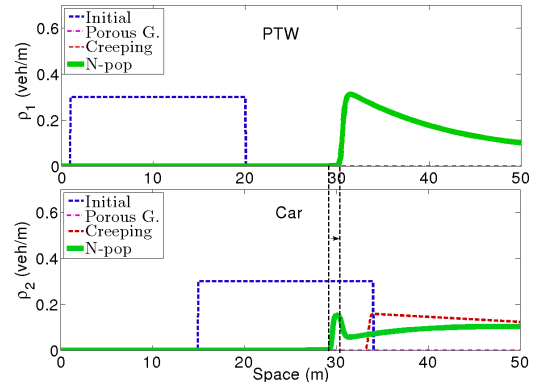
(a) Density profiles at time $t=2\text{sec}$.



(b) At time $t=18\text{sec}$, overtaking in *Porous G*

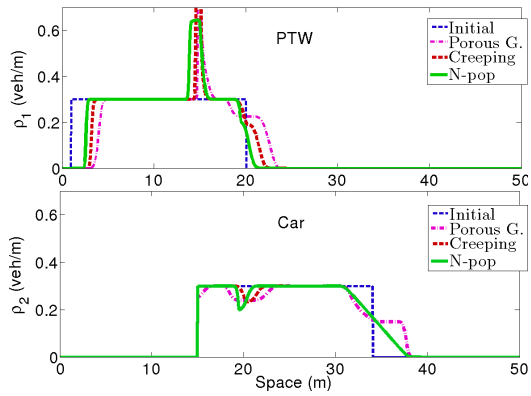


(c) At ime $t=38\text{sec}$, overtaking in *Creeping*.

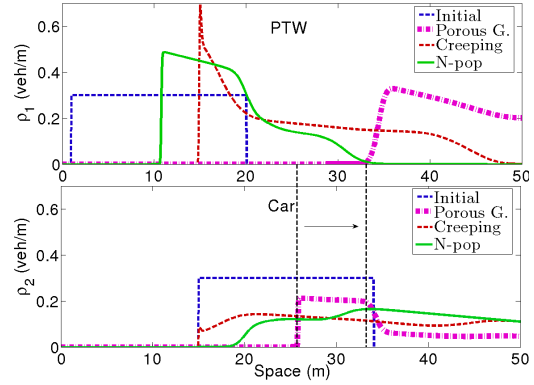


(d) At time $t=80\text{sec}$, overtaking in *N-pop*.

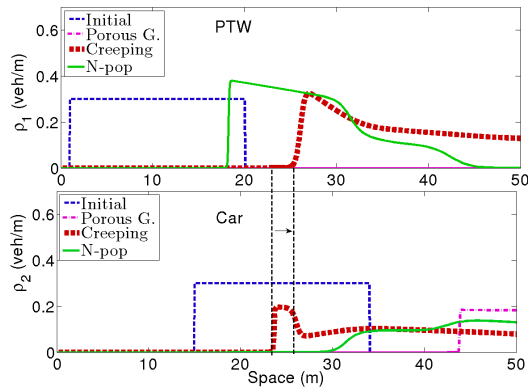
Figure 14: Overtaking experiment density-space diagrams, upper subplot for PTWs and lower subplot for cars, free flow speed of $V_1 = 1.8\text{m/s}$ greater than $V_2 = 1\text{m/s}$. The dashed lines stretching from upper subplot to the lower connect the tail of the density profiles for cars and PTWs' traffic and the spacing between the two lines indicates the distance gap after PTWs overtake.



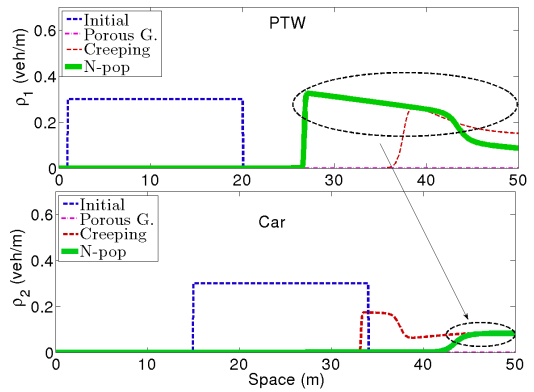
(a) Density profiles at time $t=2\text{sec}$.



(b) At time $t=26\text{sec}$, overtaking in *Porous G.*



(c) At time $t=40\text{sec}$, overtaking in *Creeping*.



(d) At time $t=52\text{sec}$, *N-pop*.

Figure 15: Overtaking experiment density-space diagrams, upper subplot for PTWs and lower subplot for cars, free flow speed of $V_2 = 1.8\text{m/s}$ greater than $V_1 = 1.5\text{m/s}$.

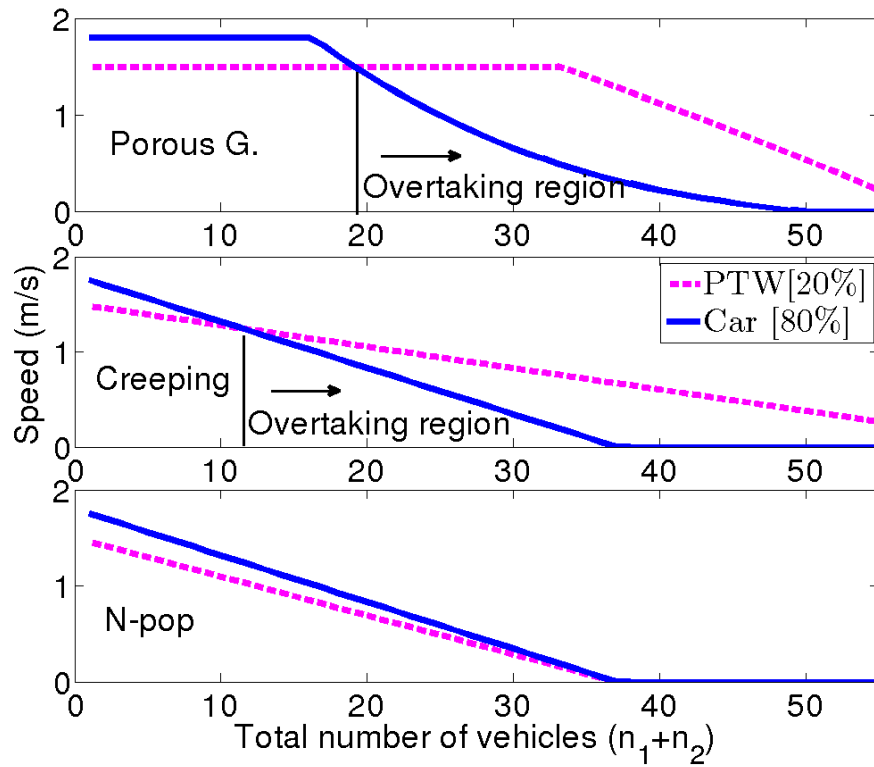


Figure 16: Speed vs. total number of vehicles plot, when free flow speed of PTWs less than cars and cars account to 80% of the total traffic, upper subplot *Porous G*, middle subplot *Creeping*, lower subplot *N-pop*.

544 tion in the composition of vehicles has no influence as long as the occupied
545 space is the same (see section 2.1, Figure 7). The *N-pop* model, however,
546 lacks the creeping behavior and overtaking is conditioned by the free flow
547 speed of PTWs.

548 4. Traffic impact analysis

549 The traffic impact analysis aims to assess the potential improvements in
550 traffic mobility obtained from growing use of PTWs. Identifying the oppor-
551 tunities leads to the introduction of new innovative smart city applications.
552 Furthermore, it gives the necessary information on how transport policies,
553 mobility plan, traffic management, etc. should be shaped to benefit from
554 the opportunities. Thus, the section here explores the impact of PTWs on
555 traffic flow, road capacity and queue discharge time. First, we analyze the
556 role of PTWs, at different penetration rates, on minimizing congestion, by
557 substituting some of the cars with PTWs. Next, we investigate how shifting
558 travel mode to PTWs could help in the reduction of travel times. Finally,
559 we study the effect of PTWs filtering behavior on queue discharging time.

560 4.1. Road capacity

561 Road capacity, which is also called critical density, is defined as the max-
562 imum volume of traffic that corresponds to the maximum flow rate. Above
563 the road capacity, traffic flow enters congestion state and the flow of vehicles
564 decreases with the increase in traffic volume. In mixed traffic flow, the road
565 capacity varies depending on the total density and the traffic composition.
566 Here, the role of PTWs in reducing congestion is evaluated. For the compar-
567 ison, the flow-density plot for different ratios of PTWs is presented in Figure
568 17. The following simulation parameters are used to produce the results.
569 The maximum speed of cars is $V_2 = 100 \text{ km/hr}$, maximum speed of PTWs
570 is $V_1 = 80 \text{ km/hr}$ and we consider a single lane one-way road with a carriage
571 width of 3.5m .

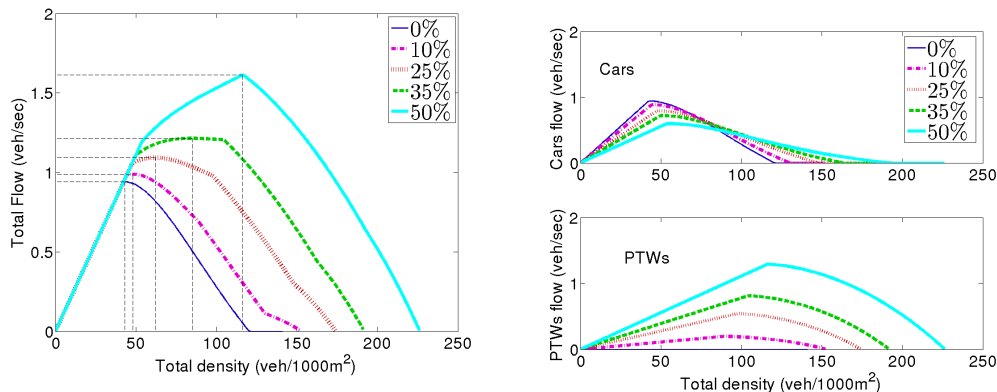
572 PTWs stay in free flow state for longer ranges of density than cars, be-
573 cause of their ability to ride in between other vehicles. The flow-density
574 diagram, which is depicted in Figure 17(b), shows the variation of maximum
575 flow rate and critical density of the two classes. Figure 17(a) shows the total
576 flow rate against the total volume of vehicles. The total flow rate describes
577 the number of vehicles that leave a given point per unit time, which in our
578 case is equal to the sum of the flow rates of PTWs and cars. As Figure 17(a)

579 illustrates, increasing the proportion of PTWs on the total traffic from 0%
 580 to 10% results in a 9.3% improvement of the road capacity and 2.74% of the
 maximum flow rate. The results in Figure 17 and Table 4 point up that shift

% of PTWs	Critical density (veh/km)	Maximum flow (veh/hr)
0	43.1	4248
10	47.1	4320
25	58.1	4608
35	72.1	4896
50	116.1	6084

Table 4: The Change in Critical Density (*veh/km* per unit lane width) and Maximum
 Flow Rate (*veh/hr/lane*) at Different Ratios of PTWs

581
 582 to PTWs indeed helps to improve road capacity. Besides, the variation on
 583 the reaction of the two traffic classes for a given traffic situation entails a
 new method for mobility management and monitoring.



(a) Total flow rate vs. total density, the
 connecting dashed lines show the
 maximum flow rate and the
 corresponding road capacity.

(b) Flow-total density diagram, upper
 subplot for cars and lower subplot for
 cars.

Figure 17: Flow-density diagram, for different penetration rates of PTWs.

584

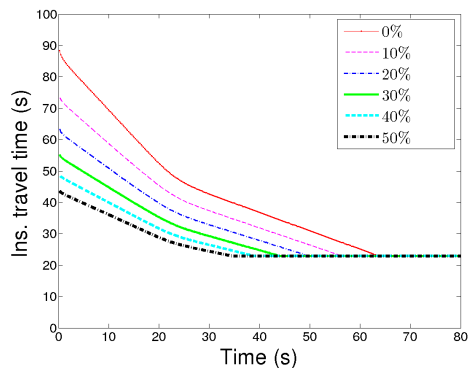
4.2. Travel time

585 Here, we analyze how replacing some of the cars with PTWs improves
 586 travel time based on the instantaneous travel time analysis. The instant-
 587

588 neous travel time (iTt) is computed on the assumption that vehicles travel
 589 through the considered road section at a speed profile identical to that of the
 590 present local speed and it is formulated as:

$$t_{inst} = \sum_{i=1}^n \frac{\Delta x}{v(x_i, t)}, \quad (21)$$

591 where n is the number of cells and Δx is the mesh size. The experiment
 592 is done under the following simulation setups: road length $500m$, $\Delta x =$
 593 $10m$, free flow speeds $V_1 = V_2 = 80km/hr$ and the simulation is run for
 594 $80sec$. A homogeneous initial total density of $\rho_1(x, 0) + \rho_2(x, 0) = 0.1$ for
 595 $x \in [0, 500m]$ is set. The result in Figure 18 is produced by computing the
 596 instantaneous travel time every $0.02sec$. According to the result, a 12.4%
 597 reduction on average travel time is obtained even at the lowest penetration
 598 of PTWs (10%). The table in Figure 18 below presents the iTT values
 599 averaged over the whole simulation period for different traffic compositions
 600 and the improvement on the average travel time. According to these results,
 601 in addition to the reduction of the average travel times, with more shift of
 602 cars to PTWs, cars travel at high speed for more time. Certainly, the results
 603 show that PTWs help in maintaining reliable and reduced travel times.



% of PTWs	cars average travel time	Improv. (%)
0	41.6	
10	36.45	12.4
20	32.74	21.3
30	30	27.9
40	28	32.7
50	26.68	35.9

Figure 18: Change in travel time of cars for different penetration rate of PTWs.

604 4.3. Queue clearance time

605 At signalized intersections, PTWs creep through the queue of other traffic
 606 to reach the front line. As more PTWs accumulate at the front of the queue,
 607 it is likely that they discharge from the queue much quicker than cars. Since

608 cars behind are forced to wait until all the PTWs in the front leave the
 609 queue, this may cause further delay on the cars clearance time. In this part,
 610 we study the effect of PTWs filtering behavior on cars traffic clearance time
 611 and the overall traffic flow.

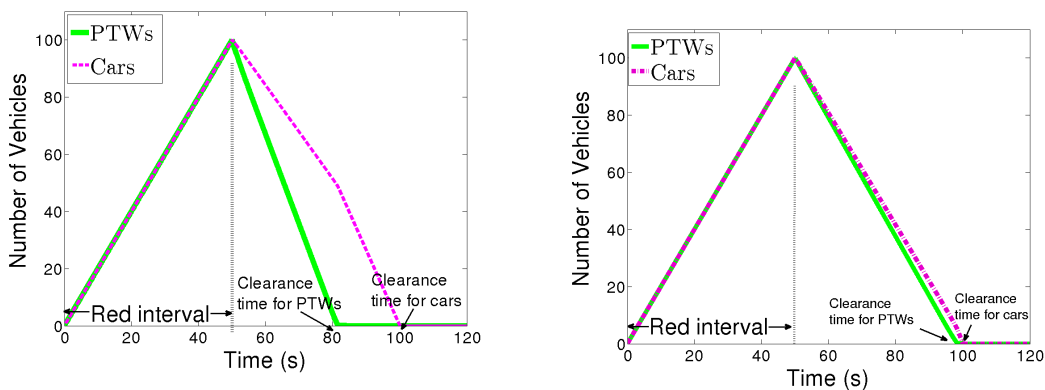
612 Queue clearance time is defined as a green time interval to exhaust the
 613 queue and it is determined by finding out the time where the number of
 614 vehicles upstream the traffic light equals zero.

$$T_c^i = \inf\{t^i : \rho_{avg}^i = 0\}, \quad i = 1, 2,$$

615 where ρ_{avg}^i represents the average density of the vehicles in the study domain.
 616 Thus, with M denoting the number of space steps in the study domain, i.e.
 617 the space before the traffic light, the average density is computed as:

$$\rho_{avg}^i = \frac{1}{M} \sum_{s=1}^M \rho_s, \quad i = 1, 2.$$

618 For the study, two simulation scenarios have been considered. First, PTWs
 619 are allowed to filter through the queue of cars traffic. On the second scenario,
 620 PTW and cars act in a similar manner, i.e. PTWs don't creep through the
 621 queue of cars traffic. The later scenario is produced by assigning the same
 critical pore size for both classes.

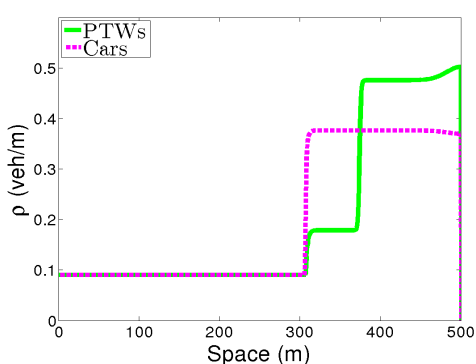


(a) Clearance time when Filtering of PTWs is allowed.

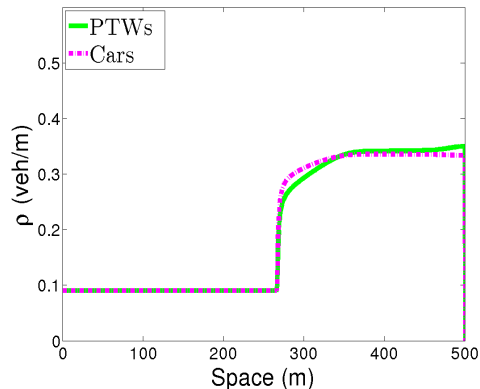
(b) Clearance time, no filtering.

Figure 19: Evolution of number of vehicles in the queue over time.

622



(a) Density profile of PTWs and cars, when PTWs are allowed to filter through traffic queue.



(b) Density profile of PTWs and cars, cars and PTWs behave in a similar manner.

Figure 20: Spatial distribution of the density of vehicles in the queue.

623 The simulation are run on the space domain $x \in [0, 5001m]$ and the
 624 inflow in the upstream direction, for both classes, is set to have the following
 625 values:

$$F_i(0, t) = \begin{cases} 2 \text{ veh/s} & \text{for } t \in [0, 50\text{sec}], \\ 0 & \text{otherwise.} \end{cases}$$

626 The traffic light (TL) is placed at $x = 500m$. The simulation starts with a
 627 red phase and stays in this state for the first 50 seconds.

628 To observe the queue clearance time and queue discharging behavior for
 629 both vehicle classes, the evolution of the number of vehicles in the queue
 630 is shown in Figure 19 and the spatial distribution of vehicles in the queue,
 631 immediately before the beginning of the green light period, is presented with
 632 the density profile plot shown in Figure 20.

633 According to the results from the first experiment, where filtering of
 634 PTWs allowed, most of the PTWs occupy the front of the queue during
 635 the queue formation (see Figure 20(a)), and they clear from the queue 28sec
 636 before cars traffic. On the other hand, no difference is observed in the clear-
 637 ance time of the two classes when PTWs are forced to behave in a similar
 638 manner to cars.

639 A comparison of the plots in Figure 20(a) with Figure 20(b) show that,
 640 with the filtering of PTWs, higher percentage of PTWs reach the front line

641 of the queue. However, PTWs attain high speed rapidly and dissipate from
642 the queue faster. As a result, there is no a significant delay incurred on cars
643 traffic because of the filtering behavior of PTWs. The message here is that
644 PTWs creeping behavior has no influence on clearance time of cars, but rather
645 improves the average delay experienced by road users at the intersections.
646 Having a facility which helps PTWs to leave first at the intersections would
647 allow better use of this opportunity offered by PTWs.

648 In general, the results indicate the positive impact of PTWs creeping be-
649 haviors on queue clearance time and the necessity to consider such behaviors
650 on the design of traffic light operation, particularly when the ratio of PTWs
651 is higher.

652 **5. Calibration of the model**

653 The model is validated against the desired qualitative behaviors. Yet, to
654 accurately reproduce the real traffic situation adjusting the model paramete-
655 rs is imperative. The model is founded on the assumption that the traffic
656 flow behavior can be characterized using the inter-vehicle spacing distribu-
657 tion. Thusly, the accuracy of the model highly depends on how precisely
658 the inter-vehicle spacing distribution is estimated. The inter-vehicle spac-
659 ing distribution, therefore, has to be calibrated from empirical data. The
660 calibration process involves, for different traffic compositions and densities,
661 collecting position information of vehicles, measuring spacing between vehi-
662 cles, estimating statistical parameters of inter-spacing (mean, variance) and
663 curve fitting experiments. Thereafter, the functional relationship of speed
664 and inter-vehicle spacing distribution should be calibrated based on real ob-
665 servation. This could be done by employing a trial and error calibration
666 method where the value of the speed function parameters, such as critical
667 pore size (gap) and jam density, are adjusted until a good fitting curve to
668 the observation is obtained. The jam and critical density values are depen-
669 dent on the actual traffic state, that is, the traffic compositions and density.
670 Therefore, it is also necessary to establish an accurate relationship between
671 the jam and critical density parameters, and the traffic state.

672 For the calibration, real trajectory data for each vehicle class and different
673 ranges of density is required. In addition, for non-lane based traffic the influ-
674 ence of the road geometry is significant, thus information about the roadway
675 such as lane width, number of lanes, etc is necessary. Although there are
676 widely available methods to collect vehicles' trajectory data, only a few of

677 them are applicable for the required validation experiment. The challenge is
678 mainly on getting the required traffic parameters and accurate geo-location
679 of vehicles, specifically PTWs. For example, data collected from sensors like
680 inductive loops are not sufficient as extrapolation of vehicles spatial location
681 is very difficult, if not impossible. Floating Car Data (FCD) could be an
682 efficient method for collecting vehicles' trajectory data, where smartphones
683 or GPS devices in vehicles continuously send location, speed, etc. infor-
684 mation. However, the inefficiency of smartphone GPS to produce the true
685 location of PTWs (Koyama and Tanaka, 2011) and the low penetration rate
686 of vehicles equipped with an accurate GPS receiver make FCD method less
687 applicable. Another potential alternative is to use video cameras and to ex-
688 tract the required traffic data (vehicle number, vehicle type, location, etc.)
689 utilizing image processing techniques (Mallikarjuna et al., 2009). Given the
690 complexity of data collection, calibrated commercial simulators like VISSIM
691 can serve as a means of model calibration. Yet, as the simulator might be
692 calibrated to a particular scenario, the model validation would be valid only
693 to that specific scenario.

694 **6. Summary and conclusion**

695 Motorcycles, scooters and other moped, thereafter referred to as Pow-
696 ered Two-Wheelers (PTWs), have peculiar maneuvering behaviors, such as
697 filtering through slow moving or stationary traffic, or lacking lane discipline,
698 which create mixed traffic flow characteristics resembling more disordered
699 flows rather than lane-based follow-the-leader flows. Mixed flow models con-
700 sidering ordered flows accordingly fail to truly represent the impact of PTW
701 on heterogeneous traffic flow characteristics. This paper specifically inves-
702 tigated disordered PTWs moving similarly to a fluid in a porous medium.
703 An enhanced mixed flow traffic model is provided, based on an innovative
704 modeling of the distribution of the pore sizes. This model is then used to
705 evaluate the impact of a gradual penetration of PTWs on mixed flow traffic
706 characteristics.

707 The close form distribution of pore size in porous media has been val-
708 idated by comparing it against typical PTW flow characteristics and also
709 benchmarked against related studies. This model allowed us to propose a
710 mathematical formulation of the fundamental relation between speed and
711 density for both cars and PTW individually. The latter aspect could be very

712 beneficial in related traffic flow studies, which assumed identical fundamental
713 relations for PTWs and cars.

714 The evaluation of the impact of PTWs on mixed traffic showed that a
715 gradual replacement of cars with PTWs manages to increase the flow capacity
716 by 9.3% already with 10% PTW penetration. The results not only confirmed
717 the benefit of PTWs in reducing travel times, but also illustrated the mutual
718 benefit of a gradual penetration of PTWs on travel times for both PTWs and
719 passenger cars (12.4 % benefit on cars at 10% penetration of PTWs). Finally,
720 we also showed that PTWs creeping through slow passenger car traffic at
721 traffic light actually impacts queue clearance time and as such should be
722 considered by traffic light where the cycles length is set according to queue
723 clearance time.

724 The presented model assumes that both classes of vehicles disregard the
725 lane discipline and their spatial distribution over the road segment follows
726 Poisson point process. As a future work, we aim to consolidate the model
727 by applying a more realistic approach for the spatial distribution and lane
728 discipline of cars. The model is validated against the desired qualitative
729 behaviors. Yet, to accurately reproduce the real traffic situation adjusting
730 the model parameters is imperative. The model parameters such as the
731 maximum speeds, jam and critical densities, stochastic characteristics of the
732 probability density function of the spacing distribution, and the fundamental
733 diagram should be tuned using real traffic data. For the calibration, the
734 traffic data collected either from field or calibrated simulation platforms can
735 be used. Because of the scarcity of real traffic data containing the trace
736 of PTWs, we will perform the model calibration using VISSIM, which is a
737 calibrated simulation platform.

738 **References**

739 Adnan, M., 2014. Passenger car equivalent factors in heterogenous traffic
740 environment-are we using the right numbers? *Procedia engineering* 77,
741 106–113.

742 Ambarwati, L., Pel, A. J., Verhaeghe, R., van Arem, B., 2014. Empirical
743 analysis of heterogeneous traffic flow and calibration of porous flow model.
744 *Transportation research part C: emerging technologies* 48, 418–436.

745 Benzoni-Gavage, S., Colombo, R. M., 2003. An n -populations model for traf-
746 fic flow. *European Journal of Applied Mathematics* 14 (05), 587–612.

- 747 Chanut, S., Buisson, C., 2003. Macroscopic model and its numerical solution
748 for two-flow mixed traffic with different speeds and lengths. *Transportation*
749 *Research Record: Journal of the Transportation Research Board* (1852),
750 209–219.
- 751 Chen, G., Meng, F., Fu, G., Deng, M., Li, L., 2013. A cell automation traffic
752 flow model for mixed traffic. *Procedia-Social and Behavioral Sciences* 96,
753 1412–1419.
- 754 Daganzo, F. C., 2002. A behavioral theory of multi-lane traffic flow. part
755 I: Long homogeneous freeway sections. *Transportation Research Part B:*
756 *Methodological* 36, 131–158.
- 757 Fan, S., Work, D. B., 2015. A heterogeneous multiclass traffic flow model
758 with creeping. *SIAM Journal on Applied Mathematics* 75 (2), 813–835.
- 759 Jiang, C., Zhang, H., Han, Z., Ren, Y., Leung, V. C., Hanzo, L., 2016.
760 Information-sharing outage-probability analysis of vehicular networks.
761 *IEEE Transactions on Vehicular Technology* 65 (12), 9479–9492.
- 762 Koyama, Y., Tanaka, T., 2011. High-precision motorcycle trajectory mea-
763 surements using gps. *SICE Journal of Control, Measurement, and System*
764 *Integration* 4 (3), 199–205.
- 765 Lenorzer, A., Casas, J., Dinesh, R., Zubair, M., Sharma, N., Dixit, V., Tor-
766 day, A., Brackstone, M., 2015. Modelling and simulation of mixed traffic.
767 In: *Australasian Transport Research Forum (ATRF), 37th, 2015, Sydney,*
768 *New South Wales, Australia.*
- 769 LeVeque, R. J., 1992. *Numerical methods for conservation laws. Vol. 132.*
770 *Springer.*
- 771 Lighthill, M., Whitham, G., 1955. On kinematic waves. i. flood movement in
772 long rivers. In: *Proceedings of the Royal Society of London A: Mathemat-*
773 *ical, Physical and Engineering Sciences. Vol. 229. The Royal Society, pp.*
774 *281–316.*
- 775 Logghe, S., Immers, L. H., 2008. Multi-class kinematic wave theory of traffic
776 flow. *Transportation Research Part B: Methodological* 42 (6), 523–541.

- 777 Mallikarjuna, C., Phanindra, A., Rao, K. R., 2009. Traffic data collection
778 under mixed traffic conditions using video image processing. *Journal of*
779 *transportation engineering* 135 (4), 174–182.
- 780 Mallikarjuna, C., Rao, K. R., 2006. Area occupancy characteristics of het-
781 erogeneous traffic. *Transportmetrica* 2 (3), 223–236.
- 782 Mathew, T. V., Munigety, C. R., Bajpai, A., 2013. Strip-based approach for
783 the simulation of mixed traffic conditions. *Journal of Computing in Civil*
784 *Engineering* 29 (5), 04014069.
- 785 Miles, R. E., 1970. On the homogeneous planar poisson point process. *Math-*
786 *ematical Biosciences* 6, 85–127.
- 787 Minh, C. C., Sano, K., Matsumoto, S., 2012. Maneuvers of motorcycles
788 in queues at signalized intersections. *Journal of advanced transportation*
789 46 (1), 39–53.
- 790 Nair, R., Mahmassani, H. S., Miller-Hooks, E., 2011. A porous flow approach
791 to modeling heterogeneous traffic in disordered systems. *Transportation*
792 *Research Part B: Methodological* 45 (9), 1331–1345.
- 793 Nair, R., Mahmassani, H. S., Miller-Hooks, E., 2012. A porous flow model
794 for disordered heterogeneous traffic streams. In: *Transportation Research*
795 *Board 91st Annual Meeting*. No. 12-3260.
- 796 Newell, G. F., 1993. A simplified theory of kinematic waves in highway traffic,
797 part i general theory, part ii: Queueing at freeway bottlenecks, part iii
798 multi-destination flows. *Transportation Research Part B: Methodological*
799 27 (4), 281–313.
- 800 Pandey, G., Rao, K. R., Mohan, D., ??? Modelling vehicular interactions for
801 heterogeneous traffic flow using cellular automata with position preference.
802 *Journal of Modern Transportation*, 1–15.
- 803 Praveen, P. S., Arasan, V. T., 2013. Influence of traffic mix on pcu value
804 of vehicles under heterogeneous traffic conditions. *International Journal of*
805 *Traffic and Transport Engineering* 3 (3), 302–330.
- 806 Richards, P. I., 1956. Shock waves on the highway. *Operations research* 4 (1),
807 42–51.

808 SHIOMI, Y., HANAMORI, T., Eng, M., Nobuhiro, U., SHIMAMOTO, H.,
809 2012. Modeling traffic flow dominated by motorcycles based on discrete
810 choice approach. In: Proceedings of 1st LATSIS Conference.

811 Van Lint, J., Hoogendoorn, S., Schreuder, M., 2008. Fastlane: New multiclass
812 first-order traffic flow model. Transportation Research Record: Journal of
813 the Transportation Research Board (2088), 177–187.

814 van Wageningen-Kessels, F., 2013. Multi-class continuum traffic flow models:
815 analysis and simulation methods. Ph.D. thesis, TRAIL.

816 Wong, G., Wong, S., 2002. A multi-class traffic flow model—an extension of
817 lwr model with heterogeneous drivers. Transportation Research Part A:
818 Policy and Practice 36 (9), 827–841.

819 Zhang, H., Jin, W., 2002. Kinematic wave traffic flow model for mixed traffic.
820 Transportation Research Record: Journal of the Transportation Research
821 Board (1802), 197–204.

822 Zhang, P., Liu, R.-X., Wong, S., Dai, S.-Q., 2006. Hyperbolicity and kine-
823 matic waves of a class of multi-population partial differential equations.
824 European Journal of Applied Mathematics 17 (2), 171–200.

825 **List of Figures**

826	1	Heterogeneous traffic flow for PTWs and cars.	7
827	2	Vehicles spacing distribution, where ρ_1 and ρ_2 represent, re- 828 spectively, PTWs and cars density	8
829	3	Delaunay triangle edges length for circles.	9
830	4	Comparison of estimated probability distribution function and 831 fitting theoretical distributions for different vehicles composition	10
832	5	Example $\rho_1 = \rho_2 = 0.03 \text{ veh}/m^2$: PDF of the inter-vehicle 833 distance on a road with dimension $L = 100$ and W ranging 834 from $5m - 100m$	12
835	6	Speed vs total occupied area for constant critical pore size 836 ($r_c^2 = 3m$) and a variable critical pore size (r_c^1) with the fol- 837 lowing parameters $r_c^{min} = 3m$ and $r = 2m$	13

838	7	Speed Vs total occupied area ($\sum \rho_1 A_1 + \sum \rho_2 A_2$), where $\rho_1 A_1$	
839		and $\rho_2 A_2$ are area projected on the road by PTW and car,	
840		respectively.	14
	8	Evaluation of the maximum characteristics speed over a point	
		in $S = \{\rho_1, \rho_2\}$, Here $V_1 = 22m/s$ and $V_2 = 27m/s$	17
	9	Evaluation of minimum characteristics speed over a point in	
		$S = \{\rho_1, \rho_2\}$, Here $V_1 = 22m/s$ and $V_2 = 27m/s$	18
841	10	<i>Normal profile</i> , traffic density waves of cars and PTWs at differ-	
842		ent time steps. (PTW-1, Car-1) and (PTW-2, Car-2) rep-	
843		resent result form our model and Nair's model, respectively. .	21
844	11	<i>Queue profile</i> , traffic density waves of cars and PTWs at differ-	
845		ent time steps. (PTW-1, Car-1) and (PTW-2, Car-2) rep-	
846		resent result form our model and Nair's model, respectively. .	22
	12	Speed Vs total occupied area ($\sum \rho_1 A_1 + \sum \rho_2 A_2$) Nair's model	
		(Nair et al., 2011), where $\rho_1 A_1$ and $\rho_2 A_2$ are area projected on the road by PTW and car, respect	
847	13	Creeping experiment density-space diagram, upper subplot for	
848		PTWs and lower subplot for cars.	25
849	14	Overtaking experiment density-space diagrams, upper subplot	
850		for PTWs and lower subplot for cars, free flow speed of $V_1 =$	
851		$1.8m/s$ greater than $V_2 = 1m/s$. The dashed lines stretching	
852		from upper subplot to the lower connect the tail of the density	
853		profiles for cars and PTWs' traffic and the spacing between the	
854		two lines indicates the distance gap after PTWs overtake. . . .	27
855	15	Overtaking experiment density-space diagrams, upper subplot	
856		for PTWs and lower subplot for cars, free flow speed of $V_2 =$	
857		$1.8m/s$ greater than $V_1 = 1.5m/s$	28
858	16	Speed vs. total number of vehicles plot, when free flow speed	
859		of PTWs less than cars and cars account to 80% of the tot-	
860		al traffic, upper subplot <i>Porous G</i> , middle subplot <i>Creeping</i> ,	
861		lower subplot <i>N-pop</i>	29
862	17	Flow-density diagram, for different penetration rates of PTWs.	31
863	18	Change in travel time of cars for different penetration rate of	
864		PTWs.	32
865	19	Evolution of number of vehicles in the queue over time.	33
866	20	Spatial distribution of the density of vehicles in the queue. . .	34

867 **List of Tables**

868	1	Goodness of the fit measures obtained from the fitting experiments for different theoretical distributions.	11
869			
870	2	Simulation Parameters	24
871	3	Speed values extracted at time $t = 50sec$ and position $x =$	
872		$39.15m$	25
873	4	The Change in Critical Density (veh/km per unit lane width) and Maximum Flow Rate ($veh/hr/lane$) at Different Ratios of PTWs	31
874			
875			
876	5	Table of Symbols And Acronym Used Along The Paper	43
877	6	The mean and variance of inter-vehicle spacing distribution for Poisson and uniform distribution assumptions. $[\rho_1, \rho_2]$ shows the traffic composition where ρ_1 and ρ_2 represent, respectively, PTWs and cars densities	44
878			
879			
880			

881 **Table of symbols**

Symbol	Meaning
PTW	Powered Two Wheelers
x	spatial location
t	time
$q_{1/2}$	flow of PTWs/cars
$\rho_{1/2}$	density of PTWs/cars
$v_{1/2}$	speed of PTWs/cars
$v_{1/2}^f$	free flow speed of PTWs/cars
i	vehicle class
R	radius of circle
l_p	length of Delaunay edge for points
l_c	length of Delaunay edge for circles

Table 5: Table of Symbols And Acronym Used Along The Paper

882 **Appendix**

883 *Spatial distribution of vehicles*

884 To distribute vehicles inside the domain, we follow the following proce-
 885 dures. Given the mean vehicle density and area of the domain, the total
 886 number of vehicles in the domain is drawn from Poisson count. Then, the
 887 vehicles are distributed uniformly and independently in the domain. Here, we
 888 are considering a heterogeneous and disordered traffic. There is no a clearly
 889 defined distribution for the spatial distribution of vehicles for disordered traf-
 890 fics. In heterogeneous traffic, the space gap (lateral and longitudinal gap)
 891 maintained by different vehicle classes widely varies. Due to this, the spacing
 892 of vehicles appears random even when vehicles are in a car following process.
 893 Therefore, even for moderate and dense traffic conditions, more randomness
 894 in vehicles inter-spacing is observed in heterogeneous traffic than in homoge-
 895 neous.

896 Applying a uniform distribution instead of a Poisson one for dense traffic
 897 condition, the only difference would be that the vehicle count will not be
 898 generated from Poisson process. We have carried out a test to compare the
 899 Poisson approach and a uniform distribution. Example results in the table
 900 below show the mean and variance of inter-vehicle spacing for the two cases,
 901 i.e. Poisson distribution and uniform distribution. As reported, the Poisson
 902 and uniform assumptions yield a closely similar results. In both cases, the
 903 variability of inter-vehicle spacing decreases with increasing traffic densities.
 904 Therefore, for the purpose of analytical simplicity we use Poisson planar
 process for the spatial distribution of vehicles.

$[\rho_1, \rho_2]$	[0.005, 0.005]	[0.02, 0.01]	[0.05, 0.02]	[0.1, 0.05]	[0.15, 0.075]
	Poisson distribution				
Mean	16.57	7.84	4.39	2.15	1.471
Variance	234.5	72.89	26.70	5.677	2.02
	Uniform distribution				
Mean	17.04	8.24	4.415	2.15	1.41
Variance	223.5	76.45	26.23	5.75	1.95

Table 6: The mean and variance of inter-vehicle spacing distribution for Poisson and uniform distribution assumptions. $[\rho_1, \rho_2]$ shows the traffic composition where ρ_1 and ρ_2 represent, respectively, PTWs and cars densities

905